Flexural behaviour of NSM CFRP laminate strip systems in concrete using stiff and flexible adhesives

José Ricardo Cruz[1], Szymon Seręga[2], José Sena-Cruz[3]*, Eduardo Pereira[4], Arkadiusz Kwiecień[5] and Bogusław Zając[6]

Abstract: This work presents the results of an experimental and numerical investigation on the flexural behaviour of reinforced concrete (RC) slabs strengthened by carbon fibre reinforced polymers (CFRP) laminates applied according to the near surface mounted (NSM) technique, using stiff and flexible adhesives. Two study variables were analysed: i) the adhesive type and ii) the existence or not of pre-cracking on the slabs. The results show a clear dependence of slab's flexural performance on the adhesive type: the use of flexible adhesive yields to 80% of the maximum load achieved with stiff adhesives. The existence of pre-damage did not affect the structural behaviour of the slabs. CFRP rupture was observed with the use of stiff adhesives while CFRP debonding has occurred with the flexible one. Finally, a higher ductility was observed when using flexible adhesive.

A numerical model was worked out and calibrated to simulate the flexural behaviour of the tested slabs. The numerical simulations showed a very good agreement with the experiments. Besides the very good predictive performance in terms of load-displacement behaviour, the numerical model also correctly reproduced the failure modes obtained in the experiments and the differences in the bonding mechanisms of slabs strengthened with the stiff and flexible adhesives. It was demonstrated that the proposed numerical model can be used in engineering practice for the analysis and design of NSM CFPR strengthening systems for existing RC structures.

Keywords: NSM, stiff and flexible adhesives, CFRP, slabs, flexural tests, numerical modelling.

[1] PhD Student, ISISE/IB-S, University of Minho, Portugal. Email address: a51314@alumni.uminho.pt
[2] Assistant Professor, Cracow University of Technology, Poland. Email address: sserega@pk.edu.pl
[3] Associate Professor, ISISE/IB-S, University of Minho, Portugal. Email address: jsena@civil.uminho.pt *Corresponding author
[4] Assistant Professor, ISISE/IB-S, University of Minho, Portugal. Email address: eduardo.pereira@civil.uminho.pt
[5] Professor of CUT, Cracow University of Technology, Poland. Email address: akwiecie@pk.edu.pl
[6] Associate Professor, Cracow University of Technology, Poland. Email address: bozajac@pk.edu.pl

1. INTRODUCTION

Repair and strengthening solutions are commonly adopted in existing reinforced concrete (RC) structures as a way to preserve and rehabilitate them. The use of Fibre Reinforced Polymers (FRP) applied according to the Near Surface Mounted (NSM) technique is one of the possibilities for strengthening existing RC structures. NSM technique is based on the insertion of the reinforcing composite material in a groove cut in the concrete cover of the element to be strengthened [1-4]. Typically, stiff and hardly deformable epoxy adhesives are used to fix the FRP to concrete. This bonding agent plays a key role on the composite action of the system, because it is mainly responsible for the stress transferring between the FRP and the concrete substrate, in both service and ultimate limit states.

There are very few studies intended at assessing the influence of the adhesive stiffness and deformability on the flexural behaviour of RC elements strengthened using the Carbon FRP (CFRP) laminate systems. Only two investigations were found, both about the EBR (Externally Bonded Reinforcement) and none about the NSM technique. Derkowski et al. [5] performed a research on the use of stiff and flexible adhesive layers of different stiffness (Young's module ranging between 2 MPa and 13 000 MPa) and deformability (ultimate strains ranging between 0.2% and 150%) for bonding CFRP laminates in the flexural strengthening of RC beams. In this investigation, RC beams were strengthened with CFRP laminates using a stiff epoxy adhesive and five types of polymer adhesives of different flexibility. The beams were monotonically tested. Regarding the results, the authors reported the advantage of using highly deformable (flexible) adhesives in external bonding (EB) of CFRP laminates to RC beams as strengthening solution, such as:

i) more uniform distribution of CFRP strains along its length and smallest deflection (mainly in the case of the middle hard flexible polymer);
ii) protection against higher stress concentration in the CFRP due to cracking, reducing the risk of CFRP failure at cracks;
iii) higher load carrying capacity of these structural elements.

Kwiecień et al. [6] tested the flexural efficiency of an innovative solution for repair and strengthening of RC structures, consisting of the simultaneous use of rigid and flexible adhesive layers with CFRP laminates externally bonded at the bottom of a RC beam, previously ruptured in a fatigue test. The results indicate that this new system increases significantly the ductility of the repaired RC beam in the post-peak behaviour and eliminates the disadvantage of brittle and rapid failure (without warning) of the composite-to-concrete-joint. Moreover, the FRP composite system with stiff epoxy adhesive, when strengthening the cracked RC concrete beam, is characterised by a brittle behaviour and vulnerability to uneven deformations generating a notch effect and stress concentrations, which does not happen with this flexible alternative bonding. Kwiecień [7] studied the bond behaviour of EB systems applied in CFRP strengthening of masonry, by using stiff (an epoxy resin) and flexible (five polyurethane polymers) adhesives in single-lap shear tests. The author concluded that the tested flexible adhesive was more effective than the stiff one. Using the flexible polyurethane adhesive PS, higher ultimate forces (of about 42%) and ultimate slips (of about 63%) were reached in comparison to the stiff adhesive. The loaded-end slip attained with the flexible adhesive was about 40 times higher than with the stiff adhesive. Thus, the shear stress in the adhesive layer was reduced by the adhesive flexibility and more evenly redistributed along the bonding length. The author concluded also that the flexible polymers protected the brittle substrate against the local shear stress concentrations at the loaded-end caused usually by stiff adhesives, which is responsible for the activation of the rapid detachment process.

The existing guidelines do not explicitly consider the influence of the adhesive type on the provisions for estimation of the flexural capacity of RC members strengthened with NSM FRP systems. D'Antino and Pisani [8] assessed the accuracy of the models proposed in four guidelines, namely ACI 440.2R-08 [9], TR 55 [10], CSA S806-12 [11] and CNR DT 200 R1/2013 [12] for the estimation of the flexural capacity of RC beams strengthened with NSM CFRP composites. From the analysis performed the authors concluded that the procedures considered in these guidelines are based on the assumption that there is no relative slip between FRP reinforcement and concrete. Moreover, only the English TR 55 establishes the limitation of the strain in the NSM reinforcement to prevent the failure of the adhesive layer.

Taking into consideration the advantages of using flexible adhesives referred by the existing literature, and the lack of experience in using these adhesives adopting the NSM technique, in the present work the following effects on the flexural behaviour of the RC slabs strengthened with the NSM CFRP technique are studied:

i) the using of different types of adhesives (stiff and flexible);

ii) the existence or not of cracks in concrete before applying the composite strengthening.

In the following sections, the experimental program is detailed and the main results obtained are presented and analysed. In the last part of this work, the numerical simulations carried out to simulate the experimental responses of the tested slabs are introduced and discussed.

2. EXPERIMENTAL PROGRAMME

2.1 Test programme

The experimental program (see Table 1) consisted on the flexural testing of seven slab specimens. The investigation involved the study of three adhesive types, namely:

i) adhesive 1 (ADH1);
ii) adhesive 2 (ADH2);
iii) adhesive 3 (ADH3).

Each adhesive type was applied in two slabs:

i) a slab without pre-cracking (U);
ii) a slab which was pre-cracked before applying the strengthening system (C).

The cross-section of CFRP laminate adopted was 1.4×20 [mm]. In this study, it was also included a control slab (without the application of the strengthening system). The generic denomination adopted for the slab specimens is SL_ADHX_Y where X represents the adhesive type (1, 2 or 3) while Y indicates the absence or presence of pre-cracking (U - Uncracked and C - Cracked). The control slab was named as SL_REF.

2.2 Slab geometry and test configuration

Figure 1 presents the geometry of the slab specimens, as well as the details of the strengthening system and test configuration adopted. The slabs have a total length of 2600 mm with a rectangular cross-section of 600×120 [mm]. The bottom steel reinforcement was composed of 4 steel bars of 8 mm diameter (4∅8), which corresponds to a longitudinal reinforcement ratio, ρ_l, equal to 0.35%, while the top steel reinforcement was composed of 3∅6. Steel stirrups of 6 mm diameter spaced of 300 mm were adopted (∅6@300). The concrete cover was equal to 20 mm at the slab top and both sides and to 25 mm at the bottom. The strengthening solution is composed of 2 CFRP laminates of 1.4×20 [mm] installed in the concrete cover according NSM technique. The main purpose of this strengthening solution was to double the load carrying capacity of control slab (SL_REF). The corresponding equivalent longitudinal steel reinforcement ratio ($\rho_{s,eq}$) is equal to 0.49%, according to Sena-Cruz et al. [2]. The grooves used for installing the CFRP laminates have a constant cross-section of 5×25 [mm]. The CFRP laminates have a total length of 2200 mm coinciding their mid length with the mid span of the slab span. The absence of CFRP reinforcements at the extremities of the slab was adopted to avoid the confinement effect provided by the supporting conditions to the reinforcing materials during the test.

A four-point bending loading test configuration was adopted to perform the quasi-static monotonic tests (see Figure 1a). The distance between supports (span length) was 2400 mm, being the shear span of 900 mm (i.e. 7.5 times the slab thickness). The slab's instrumentation included the measurement of the applied load (F) using a load cell with the maximum capacity of 200 kN and a linear error of ±0.05%. For measuring the deflection along the longitudinal axis of the slab, 5 linear variable displacement transducers (LVDT1 to LVDT5) were used: 3 LVDTs in the pure bending zone (range of ±75 mm and linearity error of ±10%) and 2 LVDTs (range of ±25 mm and linearity error of ±10%), one in each side, at mid distance between the bottom supports and the line loads. The strains in the materials composing the slabs were also assessed using strain gauges glued (see Figure 1b):

i) on bottom steel bars at mid-span (SG1 and SG2);
ii) on concrete under compression stress state at the top fibre in mid-span (SG3);
iii) on the CFRP laminates - two strain gauges were placed at mid-span (SG4 and SG5), one at the loading point (SG6) and two between the loading point and CFRP extremities (SG7 and SG8).

Two different types of strain gauges were used:

i) TML BFLA-5-3-3L for steel bars and CFRP laminates;
ii) TML PFL-30-11-3L for concrete.

The tests were conducted using a servo-controlled equipment under displacement control (controlled by the internal displacement transducer of the actuator) at a rate of 20 µm/s. During the tests the crack width evolution of 3 cracks in the pure bending zone was measured using a handheld USB microscope (VEHO VMS-004 D microscope), which has a native resolution of 640×480 pixels and magnification capacity up to 400 times. In the present study, the evolution of the crack width was monitored with a magnification factor of 20 times up to a pre-defined load in order to assure the safety of the operator.

2.3 Material characterization

In this work, the mechanical properties of concrete, stiff adhesives and steel bars were experimentally assessed while the mechanical properties of both the CFRP laminate strips and the flexible adhesive were taken from other publication, since the material came from the same batch.

All slabs composing the experimental program and the specimens used for the assessment of the concrete's mechanical properties were cast from a single batch. The following characteristics were adopted for the concrete:

i) strength class: C30/37;
ii) exposure class: XC4;
iii) maximum aggregate size: 12.5 mm;
iv) slump class: S3;
v) cement: CEM II/A-L 42,5R.

The concrete composition included 907 kg/m^3 of coarse aggregates, 915 kg/m^3 of fine aggregates, 310 kg/m^3 of cement, 4.96 kg/m^3 of admixture and a water/cement (W/C) ratio equal to 0.58. The concrete's modulus of elasticity (E_c) and compressive strength (f_c) were assessed using cylinders with diameter of 150 mm and height of 300 mm, at 28 and 110 days after casting (the latter date coincides with the date of slab's testing). The modulus of elasticity and the compressive strength were assessed according to LNEC E-397-1993:1993 [13] and NP EN 12390-3:2009 [14] recommendations, respectively. Table 2 presents the obtained results (average values).

The used steel bars are of the class A400 NR SD (Eurocode 2 [15]) according to the NP EN ISO 6892–1 [16] and their mechanical properties were assessed through uniaxial tensile tests. Three specimens were used for each diameter. Table 2 presents the average values obtained for the yield stress (f_y) and ultimate strength (f_{su}).

The CFRP laminate strips used for strengthening the slabs are produced by S&P® Clever Reinforcement Ibérica with the trademark CFK 150/2000. These CFRP laminates are composed of unidirectional carbon fibres agglutinated trough an epoxy vinyl ester resin matrix, presenting a smooth surface. The content in fibres relative to matrix is about 70% (in volume). As mentioned above, the mechanical properties of the

CFRP laminate strips were assessed in other publication – see in [17]. Table 2 presents the average values obtained for the modulus of elasticity (E_f), tensile strength (f_{fu}) and ultimate strain (ε_{fmax}).

The stiff adhesives ADH1 and ADH2 (epoxy resins), have commercial trademarks Sikadur-30 and S&P Resin 220, respectively. The flexible adhesive, ADH3, with the commercial trademark of Sika PS, is a polyurethane polymer. During its application, the stiff adhesives have shown high viscosity, while the flexible adhesive exhibited low viscosity and high flexibility after curing. The adhesives are provided by the supplier in the form of two components (Component A = resin and Component B = hardener), which need to be mixed before application according the supplier's ratios A:B of 3:1, 4:1 and 9:1 for ADH1, ADH2 and ADH3, respectively. The tensile mechanical properties of ADH1 and ADH2 were obtained by performing tests according to the ISO 527-2:2012 [18], while the mechanical properties of ADH3 were previously assessed by Kwiecień [7], also according to the ISO 527-2:2012. Table 2 presents the results obtained for the elastic modulus (E_a), tensile strength (f_a) and ultimate strain (ε_{amax}) for ADH1 and ADH2 and the values collected for ADH3. It should be noted that both stiff adhesives have shown approximately similar mechanical properties, while adhesive ADH3 has shown significantly lower modulus of elasticity and tensile strength, but much higher ultimate strain.

2.4 Specimen preparation

The preparation of the strengthened slabs included several steps, namely:

i) casting;

ii) groove's opening using a saw-cut machine with a diamond disk;

iii) pre-cracking (series "_C" only);

iv) cleaning of the grooves and CFRP laminates with compressed air and acetone, respectively;

v) application of a special primer (chemically compatible) on the groove surface (for the case of slabs using ADH3), as recommended by the supplier;

vi) application of the adhesive on turned upside down specimens: ADH1 and ADH2 were applied with the assistance of a spatula while the ADH3, due to its low viscosity, was applied by gravity (see Figure 2); and finally,

vii) introduction of the CFRP laminate in the groove and regularization of the surface.

The specimens were kept in laboratory environment for approximately one month and a half before being tested.

In the series "_C", the pre-cracking process was performed using the same test configuration used for the tests up to failure described previously. The main difference was that the pre-cracking process was performed under force control at a rate of 0.05 kN/s up to a force of 15 kN, which corresponds approximately to 2/3 of the load carrying capacity of the control slab (SL_REF). When this load level was achieved, this value of force was kept constant for 10 minutes to mark the existing visible cracks and measure the width of the cracks. During the time while the force remained constant, there was an increase on mid-span displacement due to creep. After this period, the (total) mid-span deflection was about 13 mm. Finished this task, the slabs were unloaded. Then, the slabs unstressed (but with residual deformations) were strengthened with the CFRP laminates following the procedure described at the beginning of this section.

The response of the slabs "_C" was very similar to the one obtained in the control slab. During the unloading process, it could be observed the recovery of the elastic deformation, with a remaining residual mid-span deflection of about 6 mm (44% of the observed maximum displacement) and the steel residual stain of about 0.1%.

3. EXPERIMENTAL RESULTS AND DISCUSSION

3.1 Main results

Table 3 presents the main results obtained. In this table, K_{I}, K_{II} and K_{III} represent the flexural stiffness in each of the three main representative stages, respectively: i) elastic phase, ii) cracked phase, and iii) post steel yielding phase. These parameters were determined by computing the slope of the corresponding branch using two representative points; F_{cr}, F_{y} and F_{max} correspond to the force at the cracking initiation, bottom steel yielding and maximum force, respectively, and δ_{cr}, δ_{y} and δ_{max} correspond to the mid-span displacements at F_{cr}, F_{y} and F_{max}, respectively; ε_{fmax} is the maximum strain attained in the CFRP laminate at F_{max}. The values between brackets represent the increase of load carrying capacity compared to the control slab. The ductility of each slab was also assessed through the parameter δ_{max}/δ_{y}. The ratio between the residual force (at the end of the test) and the corresponding maximum force, F_{r}/F_{max} is also included. Finally, the last column includes the observed failure modes.

Figure 3 presents the applied force *versus* mid-span displacement relationships obtained for the tested slabs. These relationships present the typical behaviour observed in RC slabs strengthened in flexure with NSM-CFRP systems. It is observed an increase in load carrying capacity due to the strengthening application. In the case where no pre-cracking was applied to the slabs, three main phases can be observed:

i) the elastic phase (I), from the beginning of the test up to the crack initiation without significant change in stiffness when compared with SL_REF, due to the reduced amount of the CFRP reinforcement utilized;

ii) the cracked phase (II), from the crack initiation up to the steel yielding, where the contribution of the CFRP reinforcement starts playing an important role;

iii) the post yielding phase (III), from the steel yielding up to the maximum load carrying capacity, where the contribution of the CFRP reinforcement is responsible for carrying the additional increments of load.

As expected, the elastic phase does not exist on the pre-cracked slabs since they were pre-cracked before the application of strengthening (see Figure 3b). It is also observed a decrease of the flexural stiffness along the test due to the increase of damage in the composing materials, as well as cracking and the degradation of the bond properties between materials (steel/concrete and CFRP/adhesive/concrete).

As stated before, similar responses were obtained during the elastic phase for all slabs, including SL_REF due to the low amount of strengthening reinforcement applied. In the cracked phase, all the strengthened slabs exhibited very similar behaviour. However, at the yielding point important differences can be observed for the different types of adhesive used: SL_ADH1 and SL_ADH2 present a higher yielding load than the SL_ADH3, regardless of the existence or not of pre-cracking. This behaviour is due to the level of slip between the CFRP and concrete occurred at this load level. This slippage is directly controlled by the stiffness of the adhesive. After yielding, slabs SL_ADH1 and SL_ADH2 exhibited an almost linear elastic behaviour. Since stiff ADH1 and ADH2 provided higher level of bond between the CFRP and concrete linked with low levels of slip, the tensile failure of CFRP was achieved. As expected, after failure of the CFRP of these slabs (SL_ADH1 and SL_ADH2) the flexural response resembles the one observed in the SL_REF. It should be noted that on slabs SL_ADH3, the third branch is different from the one observed on SL_ADH1 and SL_ADH2, with a pronounced non-linear relationship between the applied force and the deflection at mid-span. This behaviour is mainly governed by the significant amount of slip between the CFRP laminates and the concrete. Due to that, the CFRP failure did not occur. After reaching the maximum load, those deformation coincides with the deformation achieved in the slabs

SL_ADH1 and SL_ADH2 at the maximum load, a softening branch with a gradual decrease of strength is observed, with a significant residual strength (for 120 mm of deflection was about 77% of F_{max}). This more deformable response observed in SL_ADH3 can be explained by the initial higher shear deformation of the flexible adhesive and then the progressive loss of bond between the CFRP laminate and concrete, and by the progressive increasing cohesive failure at the adhesive, which decreases the contribution of the CFRP laminates for flexural capacity of these slabs after reaching the maximum load.

3.2 Strains

3.2.1 Force *versus* mid-span CFRP strain

Figure 4 presents the force *versus* mid-span CFRP strain relationships obtained for the strengthened slabs. As in force *versus* mid-span displacement relationships, three phases can be observed for uncracked series and two phases can be observed for cracked series. In general, the level of mobilization of the CFRP is higher with stiff adhesives than with flexible one, which prove the higher capacity for stress transfer of the stiff adhesives. Contrarily to SL_ADH1 and SL_ADH2, the CFRP did not fail suddenly after F_{max} on SL_ADH3, but the slow decreasing of CFRP strain can be observed after the peak load was reached. Most likely this is the result of the CFRP gradual slippage, as a consequence of the loss of bond at laminate adhesive interface. Finally, it should be noted that a smaller level of CFRP strain was attained at the initial phase of the test of the uncracked series, perhaps due to the contribution of the uncracked concrete under tension, as opposed to what was observed for the cracked series. After the crack initiation, the process of stresses transfer from the concrete under tension to the CFRP laminate results in a sudden increase of the CFRP strain when stiff adhesives are used. In contrast, in the slab where flexible adhesive was used this increase was not observed, but an almost monotonic strain increase was obtained. This may reveal a reduction of CFRP's stress concentration at the cracks locations, and the stress redistribution along the CFRP laminate provided by the flexible adhesive, leading to a smoother mobilization of the mechanical properties of the CFRP laminate as discussed in [5]. Flexible adhesive (SL_ADH3) protected the CFRP laminate against the notch effect at the crack locations, which was responsible for the CFRP laminate failure when stiff adhesives were used (SL_ADH1 and SL_ADH2).

3.2.2 Force *versus* mid-span steel strain

Figure 5 presents the force *versus* mid-span steel strain relationships for the bottom steel reinforcement. First, it should be mentioned that these results are dependent on the position of the strain gauge in relation to the concrete cracks: if a strain gauge is located in the point where a crack opens, higher values of strain are measured than if a strain gauge is placed in a zone between two cracks. The results show that:

i) for uncracked series, up to the crack initiation, the strains on steel are very small; after the crack initiation, a huge increase of the strains was observed;

ii) for the cracked series, the yielding strains are lower than the ones observed for uncracked series, probably due to the residual strain present in steel resulting from the pre-cracking process;

iii) on cracked series, the mobilization of the steel reinforcement since the beginning of the test is higher than in the uncracked series, as a result of the cracked state.

3.2.3 Force *versus* mid-span concrete strain

Figure 6 presents force *versus* mid-span concrete strain relationships. The results show that:

i) in general, SL_ADH1 and SL_ADH2 slabs presented concrete strains lower than SL_ADH3 slabs;

ii) in the transition between the elastic and cracked phase, and after steel yielding, there was a huge increase in the concrete strains, higher on SL_ADH3 than on SL_ADH1 and SL_ADH2;

iii) higher level of strains was achieved in the cracked series.

3.3 Failure modes

Figure 7 shows images of the CFRP reinforcement obtained after failure. Two types of failure modes, related to the mechanical properties of the adhesives, were observed in this study:

i) slabs SL_ADH1 and SL_ADH2 failed by rupture of the CFRP laminate at mid-span (see Figure 7a). For the SL_ADH1 and SL_ADH2 slabs, in some zones of the strengthening, it was possible to observe cracks on the adhesive-concrete interface;

ii) slabs SL_ADH3 failed by debonding of the CFRP laminate at laminate-adhesive interface, mainly at mid-span (see Figure 7b), and by cohesive failure of the adhesive on other parts along the strengthening, mainly at the ends (see Figure 7c and Figure 7d). This cohesive failure of the adhesive at the ends took place only in one laminate of each slab SL_ADH3.

3.4 Crack width, crack pattern and average crack distance

As stated in Section 2.2, the crack width of target cracks was monitored using a handheld USB microscope with a magnification factor of 20 times. To perform this, three cracks were selected on each slab in the pure bending zone: one crack as close as possible to the mid-span and the other two close to the loading points. Then, during the tests, images selected from each crack were periodically captured. For each crack image, three measurements were performed in order to obtain the average crack width. The increase in crack width due to the increase of the imposed vertical displacement was measured up to a threshold of about 30 kN of load, due to safety reasons.

Figure 8 presents the evolution of the crack width against the increase of the applied force approximately up to the steel yielding. From this stage onwards the *F*-*w* relationship stopped following the linearity observed up to this phase. The results show that, for the same load level, there is a tendency for higher crack openings on the slab SL_ADH3 than in slabs SL_ADH1 and SL_ADH2. Comparing uncracked series with the cracked series, some findings can be pointed out: the crack width measurements started earlier on the cracked series, since at the beginning of the test there were already cracks, as opposed to the uncracked series.

The final crack pattern obtained in each slab was evaluated after the test. Figure 9 presents the results obtained for both lateral and bottom surfaces of each slab. Figure 10 presents the values obtained for the average crack spacing. These results were obtained by measuring the distance between cracks at the edge between the lateral surface exposed during the test and the bottom surface.

Analysing the results, in general, strengthening leads to an:

i) increase on the number of cracks;

ii) increase on the crack band zone, which tends to extend from the pure bending zone toward the ends of the slabs (see Figure 9);

iii) and, reduction of the average crack spacing, as already observed by Correia et al. [19].

When SL_REF is used as a comparison, at the uncracked series, the reduction on the average crack spacing was about 20%, 29% e 16% respectively for the slabs SL_ADH1_U, SL_ADH2_U and SL_ADH3_U. On cracked series, the values of spacing reduction were 34%, 23% e 12%, respectively for the slabs SL_ADH1_C, SL_ADH2_C and SL_ADH3_C. The results indicate that the stiff adhesives provide higher reduction of crack spacing than the flexible one.

The crack pattern obtained for SL_ADH3 slabs was approximately similar to the one obtained for SL_REF, with higher average crack spacing than the one in slabs SL_ADH1 and SL_ADH2, as well as less increase in the number of cracks and on crack width (see Figure 9). This behaviour can be explained by the less efficient flexible adhesive on CFRP mobilisation during the test. In fact, according to the literature, the increase on the amount of the reinforcement leads to a decrease on the necessary distance for appearance of a new crack between two existing cracks. Then, once ADH3 is less efficient, the distance necessary for the formation of a new crack is higher. Thus, the crack pattern is significantly influenced by the adhesive type. The typical "fish-spine" crack pattern observed for stiff adhesives (e.g. Oehlers et al. [20]) on the concrete close to the groove of the strengthening system was also not visible in the flexible adhesive's slabs.

Comparing the uncracked and cracked series, there was a higher average crack distance on cracked series, except for SL_ADH1_C. Finally, the crack width is slightly higher in cracked series for slabs strengthened with stiff adhesive and essentially similar for slabs where the flexible adhesive was used. The number of cracks tends to be lower in cracked series.

3.5 Influence of adhesive type and pre-cracking on the flexural behaviour of the slabs

In this section, the results previously presented are analysed considering i) the force achieved at crack initiation, at steel yielding and at the maximum force, ii) maximum CFRP strain and iii) the ductility and the residual force observed in each slab.

Figure 11a presents the force recorded at crack initiation and its respective increase comparing to SL_REF. The presence of the strengthening leads to an increase in force at crack initiation in comparison to SL_REF, being observed an average increase of 42% comparing to SL_REF (see Table 3 and Figure 11). Thus, it can be concluded that at this stage, the flexural behaviour probably is not dependent of the adhesive type since they may have similar mechanical behaviour.

Figure 11b presents the force achieved at yielding phase for each slab and its respective increase compared to SL_REF. According to the results, the corresponding force was very similar on the slabs SL_ADH1 and SL_ADH2 (cracked or not), as expected. However, the slab SL_ADH1 presented a slightly higher value, perhaps due to the slightly higher mechanical properties of this adhesive. In the case of SL_ADH3, the increase of the load at this stage was smaller than with the application of the stiff adhesives. According to the values shown in Table 3 and Figure 11b, the presence of pre-cracking resulted in a decrease of 1.1%, 2.1% and 10.0% of yielding force with respect to the uncracked slabs, respectively for SL_ADH1, SL_ADH2 and SL_ADH3. From these results it can be concluded that, with the stiff adhesives, the presence of pre-cracking had little influence on the level of force reached at the yielding phase. However, when considering the flexible adhesive, this decrease was more significant. The small decrease in the yielding force observed with the stiff adhesives may be the result of a residual deflection related with internal residual strains on the bottom steel reinforcement after the pre-cracking process, which leads to slightly reduced efficiency of the strengthening.

Figure 12a shows the maximum force achieved in each slab during testing and its respective increase compared to SL_REF. Similar values of load increase were obtained for the slabs strengthened using stiff adhesives. In contrast, for the slabs where the flexible adhesive was used, the load carrying capacity was 18% smaller, for both uncracked and cracked series, than the average value reached for the slabs strengthened using stiff adhesives. Thus, a better performance was obtained with stiff adhesives, which can take better advantage of the CFRP tensile strength. On the contrary, the tensile strength was not achieved with the flexible adhesive and the CFRP slippage was observed instead of CFRP failure (see Figure 7). Comparing both series, a slight decrease of the maximum force was observed between slabs of the same adhesive. Thus, it can be concluded that the presence of cracking does not affect significantly the performance of these slabs.

Figure 12b presents the maximum CFRP strain. Higher values were obtained for slabs SL_ADH1 and SL_ADH2 than for slabs SL_ADH3 (in average, 32% higher). Regarding the influence of the pre-cracking, no significant changes in strain were observed, with decreases on SL_ADH1, SL_ADH2 and SL_ADH3 of 5.7%, 4.3% and 3.8%, respectively. Similar values of maximum strain on CFRP laminate were observed, independently of the presence of pre-cracking. This is due to the fact that, at the moment of the failure of the slab, the initial existing residual deformation/strain state have minor influence on the loading carrying capacity of the slabs, since the involved materials (concrete and steel) at the pre-cracking phase were submitted to relatively low levels of stresses. This fact can also explain the similar values obtained for the maximum force. Similar results are found in the literature, in studies where the lower influence of pre-cracking was observed (e.g. Juvandes et al. [21]). It should be highlighted that the damage applied to the slabs (pre-cracking) does not fully represent the typical conditions on existing structures, since they usually are also stressed, at least due to the self-weight. Thus, the linking of this study with a real applications should be carefully judged (e.g. the yielding of internal steel reinforcement may occur at loads lower than the ones observed in the present case).

The ductility was assessed in this study by computing the ratio δ_{max}/δ_y (see Table 3). For the uncracked series, the values obtained were quite similar, showing that the influence of the adhesive type is not significant. Comparing the two series, ductility increases on cracked series for slabs SL_ADH1, SL_ADH2 and SL_ADH3 of 7.1%, 19.5% and 43.5%, respectively, were obtained. Thus, a trend for ductility increase with pre-cracking was observed, being more pronounced for slabs SL_ADH3. Using the ratio F_r/F_{max} it is possible to show that the residual force developed by the SL_ADH3 slabs after the maximum load was significantly higher than he one for SL_ADH1 and SL_ADH2 slabs. This comparison is more significant when residual forces were compared with the maximum force of SL_REF. Using the ratio F_r/F_{max_REF} it is possible to define additional post-failure safety factor of residual load, which determines increase of post-failure slabs strength in comparison to the offered one by the steel reinforcement. For the uncracked series these increases for slabs SL_ADH1, SL_ADH2 and SL_ADH3 were of 4.0%, 8.5% and 40.2%, respectively. For the cracked series these increases for slabs SL_ADH1, SL_ADH2 and SL_ADH3 were of 12.8%, 5.6% and 44.0%, respectively. The post-failure residual load carrying capacity of the NSM CFRP system with flexible adhesive (ADH3) is pronounced, when an emergency action on a strengthened structure is considered, to safe human life and property.

4. NUMERICAL MODELLING

This section presents the numerical simulations of the experimentally tested slabs. The parameters of the model were calibrated on the basis of the experiments described in this paper and the work described in [22], where the bond-slip laws for concrete-to-laminate interface for stiff and flexible adhesives are discussed. The results obtained from the numerical simulations provide additional information on the behaviour of the structure (at a local and global level) and are a valuable supplement to the experimental tests. Additionally, the properties calibrated in the numerical model are important to support engineering practice and can be used to design and analyse NSM CFRP strengthening systems in RC existing structures.

The slabs were modelled using the DIANA FEA software [23], using material models available in the software's library.

4.1 Finite element model

The finite element mesh topology adopted in the calculations is presented in Figure 13a. The geometry of all specimens as well as loading configuration is symmetrical along the mid-span axis. Therefore, only half-span with the proper boundary conditions was modelled. The finite element mesh of the concrete matrix consists of two-dimensional quadrilateral, eight-node, isoparametric plane stress elements (CQ16M) with thickness of 600 mm in the direction perpendicular to the plane of structure. The structural type of FEM mesh was applied with the maximum dimension of each finite element of 10 mm. A three-node, two-dimensional beam element (CL9BE) with the quadratic interpolation of displacement fields was used for modelling CFRP laminate. The total cross section of the CFRP laminates used as the strengthening system was 2.8 mm in width and 20 mm in height as the two CFRP laminate of 1.4 mm width were used in the experiments. For the implemented finite element model the components of stiffness matrix and internal forces are numerically integrated over the height of its cross-section. Thus, the nonlinear effects can be modelled using this type of finite element but only in the direction parallel to the element axis (nonlinear effects are captured for stresses normal to the cross-section). This means that the model is unable to simulate the shear effects for CFRP tape as well as the effects related to partially loaded areas in the direction perpendicular to the laminate fibres, for example in the vicinity of a crack (a notch effect). However, for the NSM strengthening technique the above mentioned effects have moderate or even negligible influence on the load-displacement behaviour and the failure of the slabs. The effects of relative displacements between the laminate and the concrete matrix were modelled using zero-thickness, six-node interface elements (CL12I). The nodes of the interface, CFRP laminate and concrete elements shared the same locations. The contact perimeter of this interface element considered equal 82.8 mm, results from the two CFRP cross-section perimeters (without considering the bottom edges).

The configuration of steel reinforcement is presented in Figure 13b. The upper bars and stirrups were modelled using the concept of embedded reinforcement. This means that the reinforcement does not have its own degrees of freedom. This type of element only changes the stiffness matrix of the mother element so the uniaxial strain in the reinforcement element is compatible with the so-called mother element (i.e. an element in which reinforcement is embedded) strain fields in the direction of a bar element. The strain and stress in the embedded reinforcement are therefore calculated from the mother element strain fields.

In the case of the bottom reinforcement, local slips in the vicinity of the flexural cracks affect crack spacing, what should be reflected by the numerical model. For this reason, the bottom reinforcement is modelled using three-node truss elements connected with the concrete by special interface elements. This type of connection is able to model relative displacements (slips) between the concrete matrix and reinforcing bars in the direction tangential to the reinforcement. Similarly to the concept of embedded reinforcement, this type of slipping reinforcement can be modelled independently of the connectivity of concrete elements. In Figure 13b each line represents three ∅6 bars for the top reinforcement, two ∅6 bars for the stirrups and four ∅8 bars for the bottom reinforcement.

The effect of lack of compatibility of displacements in the horizontal direction between top and bottom surfaces of the slabs and the steel loading plate or supporting plate is reflected by the interface elements (CL12I).

4.2 Material constitutive relationships

4.2.1 Concrete model

The constitutive model of concrete applied in the numerical simulations is based on the smeared crack approach with fixed crack direction [23], [24], [25]. In this approach the nonlinear, uniaxial stress-strain relationships (Figure 14) are evaluated in the directions of the principal strains. The stiffness matrix is calculated on the basis of the secant elastic modulus $\bar{E}_{comp}$ and $\bar{E}_{tens}$, see Figure 14. Following the fixed crack concept the local directions for evaluating stress-strain relationships are "frozen" after the appearance of the first crack. In the fixed coordinate system the shear strains and stresses appear. The shear stiffness is reduced multiplying the shear modulus by a shear retention factor, $\beta < 1.0$. A secondary crack may appear only in the direction perpendicular to the first crack.

In plane stress conditions the constitutive relationship based on the secant stiffness matrix is described by the following equation [24], [25]:

$$\boldsymbol{\sigma} = \mathbf{D}_{sec}\boldsymbol{\varepsilon} \tag{1}$$

where: $\boldsymbol{\sigma} = [\sigma_n \quad \sigma_t \quad \tau_{nt}]^{\mathrm{T}}$ is the vector of stresses, $\boldsymbol{\varepsilon} = [\varepsilon_n \quad \varepsilon_t \quad \gamma_{nt}]^{\mathrm{T}}$ is the vector of mechanical strains, n and t are the directions perpendicular and tangent to the first crack, respectively. Strains $\boldsymbol{\varepsilon}$ are decomposed in the total strains (total means here mechanical strains and the ones induced by shrinkage) in the following way:

$$\boldsymbol{\varepsilon} = \boldsymbol{\varepsilon}_{tot} - \boldsymbol{\varepsilon}_{sh}, \quad \boldsymbol{\varepsilon}_{sh} = -|\varepsilon_{cs}(t)| \cdot [1 \quad 1 \quad 0]^{\mathrm{T}} \tag{2}$$

where $\varepsilon_{cs}(t)$ is the evolution in time t of the mean shrinkage strain due to cement hydration and concrete drying.

In Equation (1), the secant stiffness matrix has the form:

$$\mathbf{D}_{sec} = \begin{bmatrix} \bar{E}_n & 0 & 0 \\ 0 & \bar{E}_t & 0 \\ 0 & 0 & \beta\bar{G} \end{bmatrix} \tag{3}$$

where $\bar{E}_n$ and $\bar{E}_t$ are the secant elastic modulus in the normal and tangent directions to the first crack, respectively, $\bar{G}$ is the shear modulus. The secant values of the stiffness matrix are calculated from the uniaxial stress-strain relationships. In tension this relationship is assumed as in [26], [27] – see Figure 14:

$$\sigma_t = \begin{cases} E_c \cdot \varepsilon & 0 \le \varepsilon \le \varepsilon_{cr} \\ f_t\left(\left(1+\left(c_1\dfrac{\varepsilon-\varepsilon_{cr}}{\varepsilon_{cr}^{ult}}\right)^3\right)\cdot \exp\left(-c_2\dfrac{\varepsilon-\varepsilon_{cr}}{\varepsilon_{cr}^{ult}}\right)-\dfrac{\varepsilon-\varepsilon_{cr}}{\varepsilon_{cr}^{ult}}\left(1+c_1^3\right)\cdot\exp\left(-c_2\right)\right) & \varepsilon_{cr} < \varepsilon \le \varepsilon_{cr}^{ult} \\ 0 & \varepsilon > \varepsilon_{cr}^{ult} \end{cases} \tag{4}$$

where E_c is the mean concrete elastic modulus, the same in the elastic part in tension and compression, f_t is the concrete tensile strength, $\varepsilon_{cr} = \dfrac{f_t}{E_c}$ and the constants $c_1 = 3.0$, $c_2 = 6.93$ are taken from [27].

The mesh objectivity of the numerical solution is provided by keeping constant the fracture energy G_{ft} for a given area of a cracked element [28]. Thus, the ultimate strain ε_{cr}^{ult} is calculated as $\varepsilon_{cr}^{ult} = \varepsilon_{cr} + 5.136 \cdot \dfrac{G_{ft}}{h \cdot f_t}$, where h is the crack bandwidth. For the applied type of finite element, $h = \sqrt{A_{FE}}$ [29], where A_{FE} is the area of an individual finite element.

The fracture parameters (tensile strength f_t, fracture energy G_{ft}) were not directly measured in the experimental tests. These material parameters were calculated using correlation formulas according to [30] and [31] on the basis of the experimentally obtained compressive strength of concrete. The adopted values of material parameters of concrete are shown in Table 4.

The uniaxial stress-strain curve for concrete in compression is shown in Figure 14. The formula is defined by Equation (5), in compliance with [32]:

$$\sigma_c = \begin{cases} -f_c \dfrac{1}{3}\dfrac{\varepsilon}{\varepsilon_{ce}} & \varepsilon_{ce} < \varepsilon \le 0 \\ -f_c \dfrac{1}{3}\left(1 + 4\dfrac{\varepsilon - \varepsilon_{ce}}{\varepsilon_{c1} - \varepsilon_{ce}} - 2\left(\dfrac{\varepsilon - \varepsilon_{ce}}{\varepsilon_{c1} - \varepsilon_{ce}}\right)^2\right) & \varepsilon_{c1} < \varepsilon \le \varepsilon_{ce} \\ -f_c \left(1 - \left(\dfrac{\varepsilon - \varepsilon_{c1}}{\varepsilon_c^{ult} - \varepsilon_{c1}}\right)^2\right) & \varepsilon_c^{ult} < \varepsilon \le \varepsilon_{c1} \\ 0 & \varepsilon \le \varepsilon_c^{ult} \end{cases} \tag{5}$$

where $\varepsilon_{ce} = -\frac{1}{3}\frac{f_c}{E_c}$, $\varepsilon_{c1} = 5\varepsilon_{ce}$, f_c is the concrete compressive strength. The values of the compressive strength and elastic modulus of concrete were taken directly from the experimental tests. Similarly to the post-peak behaviour of concrete in tension, compression deformations after the peak stress show a tendency to localize to a certain zone ([33], [34], [35]). This means that the descending part of the stress-strain relationship is size dependent, and stress-displacement description is more suitable in this case than stress-strain relationship. However, it is very convenient in FEM to have the constitutive material model defined by stress-strain relationship (or by their increments), as presented in Equation (5). In order to gain the objectivity of the post-peak behaviour of concrete in compression independently of FE mesh, the ultimate compressive strain is introduced to Equation (5) in the form [32]: $\varepsilon_c^{ult} = \varepsilon_{c1} - \frac{3}{2}\frac{G_{fc}}{h \cdot f_c}$, where G_{fc} is the compressive fracture energy, *h* is the characteristic length of a finite element, assumed the same as for tension. The G_{fc} value is an additional material property and can be calculated from the post-peak stress-displacement diagram. The values for this quantity available in literature range from 10.0 to 25.0 N/mm [33], [36]. The value of G_{fc} adopted in the calculations is shown in Table 4.

4.2.2 Bond-slip model between concrete and laminate, model for reinforcing steel, CFRP laminate and concrete-to-bar bond-slip behaviour

The behaviour of the concrete-to-laminate interface is described in the work [22]. In the current analysis the average values of material parameters were used for slabs strengthened using the stiff types of the adhesives – Table 4 in [22]. In the case of the flexible adhesive the average bond-slip properties lead to an overestimation of the load bearing capacity of slabs SL_ADH3_U, SL_ADH3_C. This is caused by rheological effects – the flexible adhesive is very sensitive to the loading rate [37], as discussed in the next section of this paper. The higher the strain rate, the stiffer behaviour of polyurethane material, and also the higher the strength and ultimate strain. For lower loading rates, the opposite occurs, due to creep effect. Therefore, in the simulation of the slabs strengthened with the flexible adhesive the effective bond-slip law was employed. The adopted mechanical parameters for the bond-slip law of the flexible adhesive are shown in Table 5. Figure 15 shows the comparison between the bond-slip law obtained from direct pullout tests (DPT) for a loading rate of 5 µm/s, as presented in [22], and the effective law assumed for the flexible adhesive for the rate of slip between concrete and laminate that was realized during testing of the strengthened slabs.

The bond-slip behaviour of the tensile (bottom) reinforcement is described according to [38] and presented in Figure 16a. The bond stress t_t and the relative bar - concrete slip $\bar{u}_t$ is governed by the following exponential equation:

$$t_t = a_{nb} \cdot t_{t\max} \left(1 - \exp\left(\frac{-40 \cdot \bar{u}_t}{\varnothing} \right)^{0.6} \right) \tag{6}$$

where $t_{t\max} = 0.9 f_c^{2/3}\mathrm{MPa}$, $\varnothing$ is the diameter of the tensile reinforcement bar and a_{nb} is equal to the number of tensile bars, $a_{nb} = 4$. The mechanical parameters for this bond-slip behaviour were calculated on the basis of the concrete compressive strength given in Table 4. High penalty stiffness was assumed in the direction normal to the bar.

The constitutive model for steel is unambiguously defined by the uniaxial stress-strain relationship. The elastic-plastic with linear kinematic hardening model was assumed – Figure 16b. The mechanical parameters adopted for steel were determined on the basis of experimental tests and are summarised in Table 2.

The linear elastic behaviour of CFRP laminate was characterized by the elastic modulus, ultimate tensile strength and corresponding ultimate strain according to Table 2. After reaching the ultimate strength the short plateau is assumed (0.5‰) followed by sharp drop to zero for the next 0.5‰ – Figure 16c. It should be noticed that the adopted post-peak behaviour of the laminate does not represent the experimental observations where usually, after reaching the maximum stress, the sudden rupture takes place. The short plateau followed by descending branch were assumed in order to stabilise the numerical solution.

4.3 Strategy for numerical simulations

4.3.1 Loading

Three types of loading were tested and simulated numerically. These types of loading include: the dead weight, shrinkage of concrete and external loading in the form of concentrated forces. The loading schemes were applied in the sequences that followed the experimental loading program described in the previous sections.

The self-weight was modelled as mass forces imposed at each node of the finite element mesh. The external concentrated load was simulated in two different ways. For the pre-loaded pre-cracked slabs this load was modelled as imposed forces at the node located in the middle of the steel plates used to transmit the load to the slab. For the phase after strengthening the loading process was realized in two steps: first external forces up to approximately 80% of the ultimate load of the slabs were imposed, then the loading was switched to displacement control. The node that controlled the increments of the vertical displacement was located in the middle of the steel plate. The kinetics of shrinkage strains of concrete was assumed according to [30]. Considering that the autogenous shrinkage effects take place when the elastic properties of concrete are not fully developed, only mean drying shrinkage was accounted for. The non-uniform shrinkage distributions associated to humidity gradients over the cross-section of the slabs were neglected as the tests were performed over three months after casting. It was assumed that after this time the moisture fields were uniform, and that self-balanced stresses due to non-uniform shrinkage strains were negligible, considering the reduced thickness of the slabs.

4.3.2 Phased analysis and numerical procedure

The laboratory experiments entailed several stages that had to be precisely reflected in the numerical simulations. Therefore, a phased analysis with the incremental-iterative procedure was employed in the calculations. The following phases were considered:

- Phase I – the RC slab without strengthening. The model components that were activated in this phase consist of the concrete elements, steel reinforcement, interface between the bottom rebar elements and concrete elements and kinematic boundary conditions. The initial loads were applied sequentially: shrinkage, dead weight and pre-loading (only for pre-cracked slabs);

- Phase II – strengthening and loading to approximately 80% of the ultimate load. For this phase the CFRP laminate and concrete-to-laminate interface elements were added to the components of the model from Phase I;
- Phase III – loading until the failure. In this phase the additional kinematic support was activated on the vertical direction located in the middle of the steel plate.

All loadings were applied incrementally. For each load increment, the equilibrium between internal and external forces was verified using the Newton-Raphson procedure. For the last phase the secant BFGS (Broyden–Fletcher–Goldfarb–Shanno) iteration algorithm was applied. The Euclidian norm of displacements and residual forces vectors were used as the convergence criteria. The tolerances were referred to the initial (i.e. at the beginning of each increment) displacements and residual forces vector [23]. The tolerances were 0.01 and 0.02 for displacement norm and unbalanced forces norm, respectively.

4.4 Results of numerical simulations and validation of the model

This section includes the discussion of the results obtained for the above described numerical modelling. The main mechanical quantities measured in the experimental campaign are compared with the numerical predictions. This analysis is summarised in Table 6 and in Figure 17 to Figure 20.

Figure 17 presents the results in terms of load – mid-span displacements for slabs strengthened using the stiff adhesives. In this figure also the results for the reference, unstrengthened specimen are shown. Generally, the numerical model precisely follows experimental responses for all loading stages, i.e. before cracking, during the crack formation and after cracking has stabilized, as well as after yielding of the bottom reinforcement. Some minor discrepancies can be noticed for the pre-cracked slabs at the initial phase after strengthening and for the reference slab at the post-yielding stage. The model slightly overestimates the ultimate loads (see Table 6) as well as the mid-span displacement. This is most likely due to the effect of the local action of the vertical crack edge on the CFRP laminate, which causes the earlier rupture of the laminate (a notch effect). Due to the fact that the laminate was modelled using a beam element, such local effects cannot be correctly simulated. It should be noted, however, that the discrepancies caused by these effects are less than 4% and are not important from the point of view of this numerical study.

The load-displacement responses for the slabs strengthened with the flexible adhesive are shown in Figure 18. The numerical simulations were performed for two concrete-to-laminate bond-slip models: the average obtained from the DPT tests [22] and the effective model (see Figure 15). It is demonstrated that for the average concrete-to-laminate bond-slip law the numerical model overestimates stiffness after yielding of the bottom reinforcement and the ultimate load both for the uncracked and pre-cracked slabs. This is the result of the different slip rates between the concrete and laminate applied in the DPT tests, and for this reason the average bond-slip model was adopted using the slip rate obtained in the tests on slabs SL_ADH3_U and SL_ADH3_C. The slip rate between the laminate and concrete for these two tests are compared in Figure 19. This figure shows the averaged slip rates over the total length of the CFRP laminate as a function of the mid-span displacement. It can be noticed that the slip rates are approximately one order of magnitude lower than the slip rate adopted in the DPT tests for the flexible adhesive. As mentioned in the preceding paragraph, the constitutive relationships for the flexible adhesive are very sensitive to the load rate [37]. These rheological effects were not directly taken into account mainly due to the lack of experimental data on the rheological behaviour of the flexible adhesives in the DPT tests. Therefore, the simplified approach was applied in the calculations based on the effective bond-slip concrete-to-laminate model. This model was worked out by a trial-and-error procedure and is presented in Figure 15. The results of the simulations for effective bond-slip model are in very good agreement with the experimental measurements up to the ultimate load – see Figure 18. After reaching the maximum value of the external load the simulations became unstable and did not converge to the solution. Therefore, the post critical behaviour of SL_ADH3_U and SL_ADH3_C slabs is not reflected in Figure 18.

Figure 20 presents the experimentally and numerically obtained crack pattern for SL_ADH2_U specimen. The cracks in Figure 20b are presented in the form of short lines perpendicular to the direction of the strain ε_n, and these are perceived as numerical cracks. For each finite element only one line section may be formed, representing the maximum value of ε_n from all integration points in the finite element. It should be noted that the line sections in Figure 20b are visible if the cracks have the width greater than 0.05 mm, i.e. if $\varepsilon_n \cdot h > 0.05\,\text{mm}$. The first numerical cracks appeared near the stirrups. After cracking stabilisation two to four new cracks appeared between stirrups, which were also observed during the experiments. Therefore, it can be concluded that the numerical model correctly reproduced the spacing between cracks observed experimentally, what is especially important for the simulation of bonding of the laminate between the adjacent cracks.

The beams strengthened using the stiff and flexible adhesives showed different slips and bond stress distributions along the laminate – Figure 21. For the specimens strengthened with the stiff adhesive the local anchorage of the laminate near each crack is observed. Due to the high bond strength this form of slip and bond stress development remained until the rupture of the laminate. In the case of the flexible concrete-to-laminate connection the slip and bond stress are smoother over the length of the tape. Therefore, despite the low maximum bonding strength, the laminate is able to carry stresses in the vicinity of the critical cross-sections and contribute to the stiffness of the element after yielding of the bottom reinforcement.

5. CONCLUSIONS

This paper presents an experimental and numerical research on the flexural behaviour of strengthened slabs using the NSM CFRP system and considering the following variables: (i) type of adhesive to fix the CFRP laminate to concrete (stiff and flexible adhesives) and (ii) presence or absence of cracking due to pre-loading. From this study, the following conclusions can be pointed out:

- The application of the strengthening increases the load carrying capacity of the slabs;
- For the uncracked series, the cracking load is not influenced by the adhesive type;
- During yielding, the load is dependent of the adhesive type, being 16% higher for stiff adhesives in the uncracked series and 28% in the cracked ones, when compared to the flexible adhesive;
- The two stiff adhesives resulted in similar load carrying capacities, which were 23% higher than the one obtained when using the flexible adhesive;
- The responses of slabs with stiff and flexible adhesives obtained in both uncracked and cracked series are similar, except during the elastic phase since cracked series does not show an elastic phase;
- Two distinct failure modes were observed depending on the adhesive type. When using stiff adhesives the slabs failed by the CFRP rupture, while when using the flexible adhesive the slabs failed by debonding of the CFRP;
- When using the flexible adhesive, after the maximum load the CFRP continues to contribute to the load carrying capacity, no rupture occurs and the adhesive continues to provide resistance - post failure residual load carrying capacity, about 40% higher than the residual load carrying capacity assured by steel reinforcement (additional post failure safety);

- Wider cracks are observed when flexible adhesive is used (an increase of about 50% when compared to the case of stiff adhesive);
- The crack width is shorter using the flexible adhesive (around 10%), the number of cracks observed is smaller (around 29%) and the average crack spacing is higher (around 18%) than in the case of using stiff adhesives;
- In general, the flexible adhesive provides slightly lower load carrying capacity values (around 19% less, when compared with the case where stiff adhesives are used), but it can provide a more ductile failure and a higher residual load capacity after failure (around 61% more);
- It should be noticed that numerical model precisely reflects all loading stages for the slabs strengthened with the stiff adhesives. The maximum discrepancies between the experiments and calculations are less than 4%;
- The good agreement between the model and the experimental results is also confirmed for the slabs strengthened with the polyurethane adhesive. It was demonstrated that the slip rates between concrete and laminate play a very important role in behaviour of this type of adhesive. The numerical simulations performed for the average bond-slip law, obtained from the DPT tests that were carried out for the slip rate of 5 μm/s, overestimate the load bearing capacity, because the derived average slip rate between concrete and laminate during the real tests on slabs was one order of magnitude lower (0.4μm/s). This indicates that the rheological effects have to be considered in the modelling of the bond-slip behaviour for polyurethane types of adhesives. In the presented simulations the simplified approach with the effective bond-slip model was proposed. The calculations with this effective model precisely simulate the experiments up to the failure load. Due to the numerical instabilities the model was not able to simulate the post-critical behaviour of the slabs;
- Despite the low bond strength of the flexible adhesive (in comparison with the stiff ones) the performance of the flexible strengthening system was quite satisfactory. Due to the compliance of the adhesive the concrete-to-laminate connection exhibits higher effective anchorage length with the smooth bond stress distribution along the laminate. Therefore, the laminate carries high stresses in the vicinity of the critical cross-sections and is able to contribute to the stiffness of the slabs after yielding of the bottom reinforcement. Tests of the flexible adhesives with longer anchorage lengths are required.

ACKNOWLEDGEMENTS

This work was supported by FEDER funds through the Operational Program for Competitiveness Factors – COMPETE and National Funds through FCT (Portuguese Foundation for Science and Technology) under the project FRPLongDur POCI-01-0145-FEDER-016900 (FCT PTDC/ECMEST/1282/2014) and partly financed by the project POCI-01-0145-FEDER-007633. The first and third authors acknowledge the grants SFRH/BD/131259/2017 and SFRH/BSAB/150266/2019 provided by FCT, respectively, financed by European Social Fund and by national funds through the FCT/MCTES. Finally, the authors also like to thank the S&P Clever Reinforcement Ibérica Lda. and SIKA companies for providing the materials.

REFERENCES

[1] Sena-Cruz J, Barros J, Bianco V, Bilotta A, Bournas D, Ceroni F, et al. NSM Systems. In: Pellegrino C, Sena-Cruz J, editors. Design Procedures for the Use of Composites in Strengthening of Reinforced Concrete. RILEM State-of-the-Art Reports 19, Chapter 8, 2015. p. 303-48.

[2] Sena-Cruz JM, Barros JAO, Coelho MRF, Silva LFFT. Efficiency of different techniques in flexural strengthening of RC beams under monotonic and fatigue loading. Construction and Building Materials. 2012;29:175-82.

[3] Al-Saadi NTK, Mohammed A, Al-Mahaidi R, Sanjayan J. Performance of NSM FRP embedded in concrete under monotonic and fatigue loads: state-of-the-art review. Australian Journal of Structural Engineering. 2019;20(2):89-114.

[4] Zhang SS, Yu T, Chen GM. Reinforced concrete beams strengthened in flexure with near-surface mounted (NSM) CFRP strips: Current status and research needs. Composites Part B: Engineering. 2017;131:30-42.

[5] Derkowski W, Kwiecień A, Zając B. CFRP strengthening of bent RC beams using stiff and flexible adhesives. Thecnical Transactions. Civil Engineering. 1-B/2013. Conference, Conference 2013.

[6] Kwiecień A, Derkowski W, Zając B. Protection against brittle damage of concrete structure strengthened with CFRP laminates using flexible adhesive - Laboratory test. Conference, Conference 2012.

[7] Kwiecień A. Stiff and flexible adhesives bonding CFRP to masonry substrates—Investigated in pull-off test and Single-Lap test. Archives of Civil and Mechanical Engineering. 2012;12(2):228-39.

[8] D'Antino T, Pisani MA. Evaluation of the effectiveness of current guidelines in determining the strength of RC beams retrofitted by means of NSM reinforcement. Composite Structures. 2017;167:166-77.

[9] ACI. Guide for the design and construction of externally bonded FRP systems for strengthening concrete structures. ACI 440.2R-08. American Concrete Institute Farmington Hills (MI). 2008.

[10] Society TC. Technical Report 55, Design guidance for strengthening concrete structures using fibre composite materials. 3rd edition, Crowthorne, UK: The Concrete Society. 2012.

[11] CSA. CSA S806-12, Design and construction of building structures with fibrer einforced polymers. Toronto, Canada: Canadian Standards Association. 2012.

[12] CNR. CNR. CNR-DT 200 R1/2013. Guide for the design and construction of externally bonded FRP systems for strengthening existing structures. 2013.

[13] LNEC. Concrete – determination of the elasticity young modulus under compression. E397-1993. Portuguese specification from LNEC. 1993.

[14] NP EN 12390-3. Testing Hardened Concrete. Part 3: Compressive Strength of Test Specimen. Instituto Português da Qualidade (IPQ). Caparica, Portugal. 2011.

[15] NP EN EN 1992-1-1. Eurocode 2: design of concrete structures - Part 1-1: general rules and rules for buildings. Instituto Português da Qualidade (IPQ). Caparica, Portugal. 2010.

[16] NP EN ISO 6892–1. Metallic materials. Tensile testing. Part 1: method of test at room temperature. Instituto Português da Qualidade (IPQ). Caparica, 2012.

[17] Sena-Cruz J, Jorge M, Branco JM, Cunha VMCF. Bond between glulam and NSM CFRP laminates. Construction and Building Materials. 2013;40:260-9.

[18] ISO 527-2. Plastics—Determination of Tensile Properties. Part 2: Test Conditions for Moulding and Extrusion Plastics; International Organization for Standardization (ISO): Genève, Switzerland, 2012.

[19] Correia L, Teixeira T, Michels J, Almeida JAPP, Sena-Cruz J. Flexural behaviour of RC slabs strengthened with prestressed CFRP strips using different anchorage systems. Composites Part B: Engineering. 2015;81:158-70.

[20] Oehlers DJ, Rashid R, Seracino R. IC debonding resistance of groups of FRP NSM strips in reinforced concrete beams. 2008;22:1574-82.

[21] Juvandes LFP, Dias SJE, Figueiras JA. Experimental behaviour of concrete slabs strengthened with CFRP systems. In: Proceedings of International Conference Composites in Construction (CCC2001). Conference, Conference 2001. p. 479-85.

[22] Cruz JR, Sena-Cruz J, Rezazadeh M, Seręga S, Pereira E, Kwiecień A, et al. Bond behavior of NSM CFRP laminate strip systems in concrete using stiff and flexible adhesives. Manuscript submitted to Composites Part B. 2019.

[23] TNO DIANA BV. DIANA. User's manual.

[24] Vecchio FJ. Nonlinear finite element analysis of reinforced concrete membranes. ACI Structural Journal. 1989;86(1):26-35.

[25] Vecchio FJ. Reinforced Concrete Membrane Element Formulations. Journal of Structural Engineering. 1990;116(3):730-50.

[26] Cornelissen HAW, Hordijk DA, Reinhardt HW. Experimental determination of crack softening characteristics of normalweight and lightweight concrete. Heron. 1986;31(2):45–56.

[27] Hordijk DA. Local Approach to Fatigue of Concrete. PhD thesis. Delft University of Technology. 1991.

[28] Borst Rd. Smeared cracking, plasticity, creep and thermal loading - a unified approach. Computer Methods in Applied Mechanics and Engineering. 1987;62(1):89–110.

[29] Rots JG. Computational modeling of concrete fracture. PhD thesis. Delft University of Technology. 1988.

[30] EN 1992-1-1. Eurocode 2: Design of concrete structures - Part 1-1: General rules and recommendations for buildings. CEN - European Committee for Standardization. 2004.

[31] FIB. Fib Model Code for Concrete Structures 2010. Federation internationale du beton. Ernst & Sohn, a Wiley brand; 2013.

[32] Feenstra FH, Borst R. Aspects of robust computational modeling for plain and reinforced concrete. Heron. 1993;38(4):3-76.

[33] Jansen DC, Shah SP. Effect of Length on Compressive Strain Softening of Concrete. Journal of Engineering Mechanics. 1997;123(1):25-35.

[34] Markeset G, Hillerborg A. Softening of concrete in compression - Localization and size effects. Cement and Concrete Research. 1995;25(4):702-8.

[35] Mier JGMv, Shah SP, Arnaud M, Balayssac JP, Bascoul A, Choi S, et al. Strain-softening of concrete in uniaxial compression. Materials and Structures. 1997;30(4):195-209.

[36] Vonk RA. Softening of concrete loaded in compression. PhD thesis. Eindhoven University of Technology. 1992.

[37] Kwiecień A, Gams M, Rousakis T, Viskovic A, Korelc J. Validation of a New Hyperviscoelastic Model for Deformable Polymers Used for Joints between RC Frames and Masonry Infills. Engineering Transactions. 2017;65(1):113-21.

[38] Shima H, Chou LL, Okamura H. Micro and Macro Models for Bond in Reinforced Concrete. Journal of the Faculty of Engineering, The University of Tokyo (B). 1987;22:133-94.

LIST OF TABLES

Table 1 – Experimental program.

Slab's denomination	**Type of adhesive**	**Pre-cracking**	**CFRP cross-section geometry, $t_f \times w_f$** [mm]
SL_REF	--	--	--
SL_ADH1_U	Adhesive 1 (ADH1)	No	1.4×20
SL_ADH1_C		Yes	
SL_ADH2_U	Adhesive 2 (ADH2)	No	
SL_ADH2_C		Yes	
SL_ADH3_U	Adhesive 3 (ADH3)	No	
SL_ADH3_C		Yes	

Table 2 – Material characterization (average values).

Concrete

Curing age	E_c [GPa]	f_c [MPa]
28 days	27.0 (0.5%)	35.4 (4.8 %)
110 days	28.3 (2.5%)	38.5 (2.1%)

Steel

Steel bar diameter	f_y [MPa]	f_{ts} [MPa]
∅6	631.6 (3.4 %)	781.0 (2.4 %)
∅8	546.8 (5.3 %)	669.1 (5.6 %)

CFRP

Cross-section geometry [mm]	E_f [GPa]	f_f [MPa]	ε_{fmax} [$\times 10^{-3}$]
1.4×20[a]	161.8 (0.9%)	2784.0 (3.9%)	1.7 (3.0%)

Adhesive

Type of adhesive	E_a [GPa]	f_a [MPa]	ε_{amax} [$\times 10^{-3}$]
ADH1	11.7 (0.51%)	25.6 (7.40%)	3.0 (10.91%)
ADH2	7.6 (6.15%)	17.2 (5.43%)	2.5 (13.16%)
ADH3[b]	0.008	2.2	450.0

Notes:

The values in brackets are the corresponding coefficients of variation (CoV).

[a] Results collected from [17].

[b] Results collected from [7].

Table 3 – Main results obtained from the flexural slab tests.

Slab's denomination	**Flexural stiffness**			**Crack initiation**		**Yielding**		**Maximum**			**Ductility parameter**	**Residual force ratio**	**FM**
	K_{I}	K_{II}	K_{III}	δ_{cr}	F_{cr}	δ_{y}	F_{y}	$\delta_{\max}$	$F_{\max}$	$\varepsilon_{f\max}$	$\delta_{\max}/\delta_{\mathrm{y}}$	$F_{\mathrm{r}}/F_{\max}$	--
	[kN/mm]			[mm]	[kN]	[mm]	[kN]	[mm]	[kN]	$[10^{-3}]$	[-]	[%]	--
SL_REF	7.75	0.78	0.01	0.71	7.57	20.17	21.47	158.43[a]	23.56[a]	-	-	-	-
SL_ADH1_U	9.57	1.10	0.40	1.25	10.86 (43%)	21.85	31.93 (49%)	74.04	52.87 (124%)	12.06	3.39	46.36	F
SL_ADH2_U	8.95	1.07	0.41	1.35	10.52 (39%)	22.47	31.11 (45%)	74.95	52.08 (121%)	12.49	3.34	49.10	F
SL_ADH3_U	7.94	1.28	0.34	1.58	10.86 (43%)	20.79	27.35 (27%)	72.24	42.71 (81%)	8.46	3.47	77.33	D
SL_ADH1_C	6.30[b]	1.92	0.41	1.32[b]	7.16[b]	18.95	31.58 (47%)	68.87	51.53 (119%)	12.46	3.63	51.56	F
SL_ADH2_C	6.03[b]	1.91	0.40	0.99[b]	7.78[b]	17.36	30.47 (42%)	69.33	51.06 (117%)	12.02	3.99	48.73	F
SL_ADH3_C	5.38[b]	1.81	0.34	1.06[b]	6.18[b]	13.97	24.61 (15%)	69.54	41.82 (78%)	8.33	4.98	80.13	D

Notes:

FM = Failure modes: F = CFRP failure; D = Debonding of the CFRP laminate due to cohesive failure of the adhesive; the force F_{r} corresponds to a 90 mm of mid-span vertical displacement for slabs SL_ADH1 and SL_ADH2 and 120 mm for slabs SL_ADH3; the values between parentheses represent the increase in load carrying capacity in each phase compared to SL_REF.

[a] Maximum value reached during the test without failure of the slab (by concrete crushing or failure of the longitudinal tensile steel bars).

[b] Values obtained from the pre-cracking phase (see Section 2.4).

Table 4 – Mechanical properties of concrete adopted in calculations.

E_c [GPa]	ν [-]	f_c [MPa]	f_t [MPa]	G_{ft} [N/mm]	G_{fc} [N/mm]	β [-]
28.3	0.2	38.5	2.9	0.14	25.0	0.15

Table 5 – Effective mechanical parameters for flexible adhesives.

s_1 [mm]	s_2 [mm]	s_3 [mm]	τ_m [MPa]	τ_f [MPa]	α [-]
1.5	1.6	2.4	1.3	0.6	0.5

Table 6 – Experimental vs predicted cracking, yielding and ultimate loads.

	SL_REF	**SL_ADH1_U**	**SL_ADH1_C**	**SL_ADH2_U**	**SL_ADH2_C**	**SL_ADH3_U**	**SL_ADH3_C**
$F_{cr.exp}$ [kN]	7.6	10.9	7.2	10.5	7.8	10.9	6.2
$F_{cr.num}$ [kN]	9.6	10.1	9.6	10.1	9.6	9.6	9.6
$\frac{F_{cr.exp}}{F_{cr.num}}$ [-]	0.79	1.08	0.75	1.04	0.81	1.14	0.65
$F_{y.exp}$ [kN]	21.5	31.9	31.6	31.1	30.5	27.4	24.6
$F_{y.num}$ [kN]	21.1	31.7	31.9	31.7	31.9	27.0	25.5
$\frac{F_{y.exp}}{F_{y.num}}$ [-]	1.02	1.01	0.99	0.98	0.96	1.01	0.96
$F_{max.exp}$ [kN]	23.6	52.9	51.5	52.1	51.1	42.7	41.8
$F_{max.num}$ [kN]	27.6	54.3	53.2	54.3	53.2	42.9* 54.9**	43.0* 54.9**
$\frac{F_{max.exp}}{F_{max.num}}$ [-]	0.86	0.97	0.97	0.96	0.96	0.99* 0.78**	0.97* 0.76**

Notes:

exp=Experimental; *num*=Numerical modelling

*values calculated for effective bond-slip law

**values calculated for average bond-slip law

LIST OF FIGURES

Figure 1 – Geometry, reinforcement and strengthening detailing, test configuration, and instrumentation of the slabs: (a) lateral view; (b) elevation; (c) cross section; (d) groove' details; (e-f) photos during the execution of tests. Note: all dimensions are in millimetres.

Figure 2 – Application of the adhesive: (a) Adhesive 1; (b) Adhesive 2; (c) Adhesive 3.

Figure 3 – Force *vs.* mid-span displacement obtained on the cracked (a) and uncracked (b) series.

Figure 4 – Force *vs.* mid-span CFRP strain obtained on the (a) uncracked and (b) pre-cracked series.

Figure 5 – Force *vs.* mid-span steel strain obtained on the (a) uncracked and (b) pre-cracked series

Figure 6 – Force *vs.* mid-span concrete strain obtained on the (a) uncracked and (b) cracked series.

Figure 7 – Failure modes: (a) CFRP laminate failure (SL_ADH1 and SL_ADH2); (b) debonding at laminate-adhesive interface (SL_ADH3); (c) cohesive failure of ADH3 at the ends of the strengthening system (SL_ADH3); (d) cohesive failure of the adhesive between the mid-span section and the ends of the strengthening (SL_ADH3).

Figure 8 – Crack width evolution on the (a) cracked and (b) uncracked series.

Figure 9 – Crack pattern of each slab after the test on lateral and bottom surfaces. Notes: on reference and uncracked slabs, the cracks were marked using black colour; on the cracked slabs, the cracks caused by the pre-cracking process were marked with red colour and the cracks resulting of the test up to failure were marked using black colour.

Figure 10 – Average crack distance of each slab.

Figure 11 – Force at: (a) crack initiation; (b) bottom steel yielding. Notes: the values between parentheses are the percentage increase to SL_REF at this phase of the test.

Figure 12 – Maximum force (a) and maximum CFRP strain (b). Note: the values between parentheses are the percentage increase to SL_REF at this phase of the test.

Figure 13 – Finite element model adopted for the simulation of the slabs: (a) concrete and laminate, (b) steel reinforcement.

Figure 14 – Uniaxial stress-strain relationship for concrete.

Figure 15 – Comparison of bond-slip laws for Adhesive 3, average according to DPT (red line) [22], effective (black line).

Figure 16 – (a) bond-slip law for steel reinforcement, (b) stress-strain relationship for steel reinforcement, (c) stress-strain relationship for CFRP laminate.

Figure 17 – Comparison between experimental and numerical modelling of the load *vs*. displacement behaviour for slabs with stiff adhesives: (a) slabs uncracked before strengthening, (b) slabs preloaded and cracked before strengthening.

Figure 18 – Comparison between experimental and numerical modelling of the load *vs*. displacement behaviour for slabs with flexible adhesive: (a) slab uncracked before strengthening, (b) slab preloaded and cracked before strengthening.

Figure 19 – Averaged slip rate between CFRP laminate and concrete for SL_ADH3_U slab.

Figure 20 – Comparison between the experimental and numerical crack pattern for slab SL_ADH2_U.

Figure 21 – Development of slips (a), (c) and bond stresses (b), (d) for slabs SL_ADH1_U (stiff adhesive) and SL_ADH3_U (flexible adhesive) – external load of 40 kN.

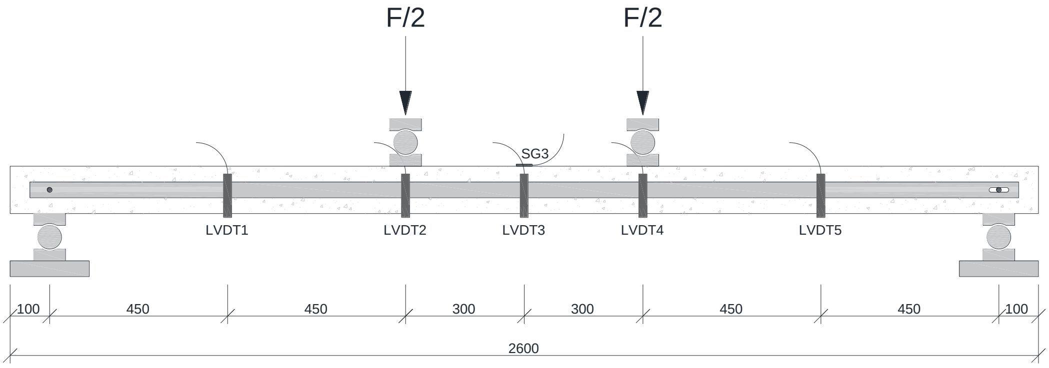

(a)

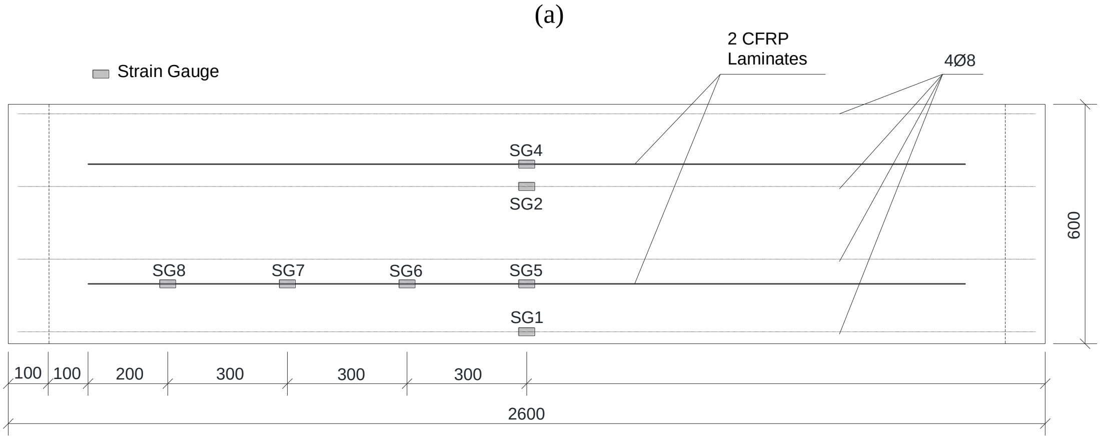

(b)

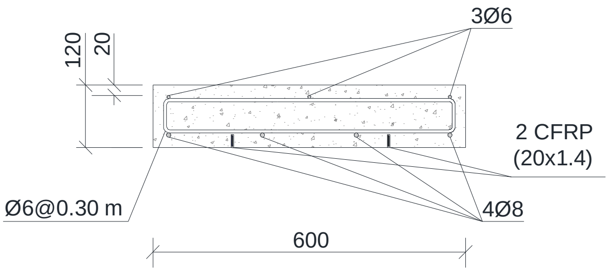

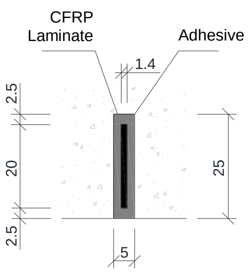

(c) (d)

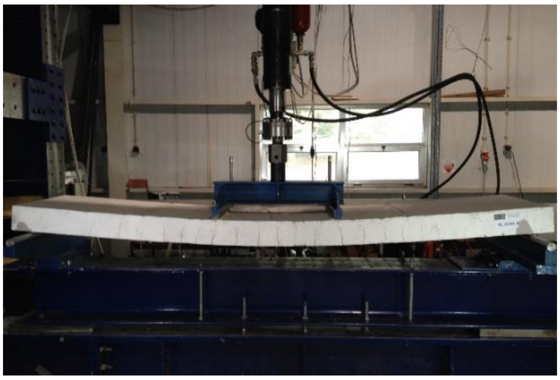

(e) (f)

Figure 1 – Geometry, reinforcement and strengthening detailing, test configuration, and instrumentation of the slabs: (a) lateral view; (b) elevation; (c) cross section; (d) groove' details; (e-f) photos during the execution of tests. Note: all dimensions are in millimetres.

(a) (b) (c)

Figure 2 – Application of the adhesive: (a) Adhesive 1; (b) Adhesive 2; (c) Adhesive 3.

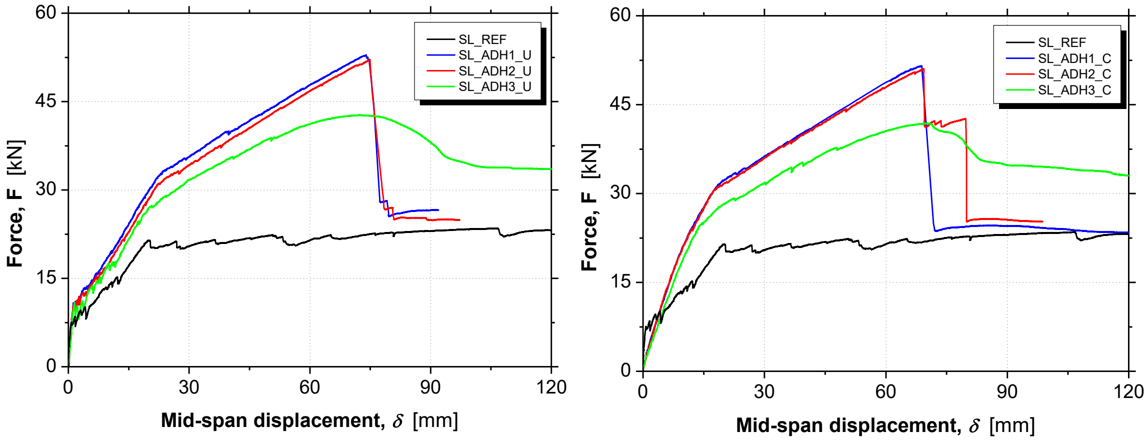

(a) (b)

Figure 3 – Force *vs.* mid-span displacement obtained on the cracked (a) and uncracked (b) series.

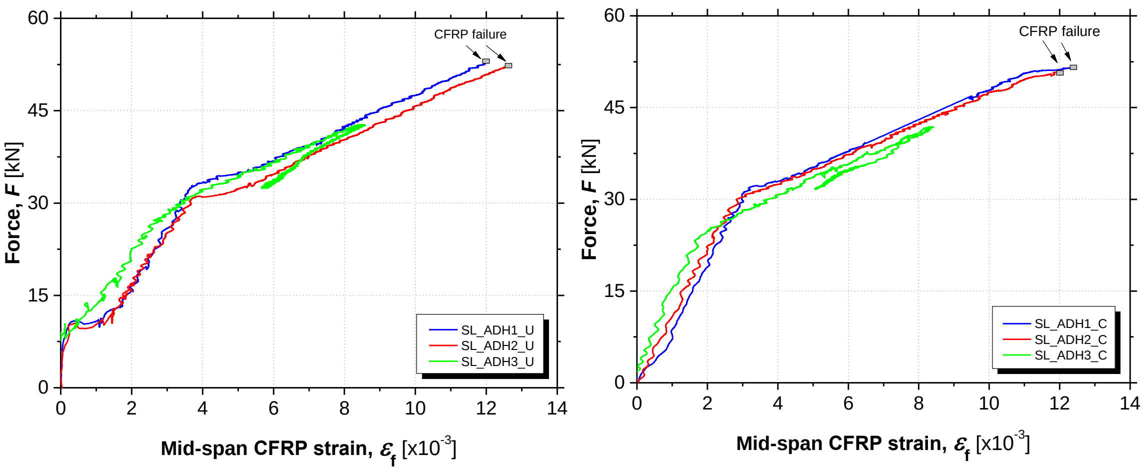

(a) (b)

Figure 4 – Force *vs.* mid-span CFRP strain obtained on the (a) uncracked and (b) pre-cracked series.

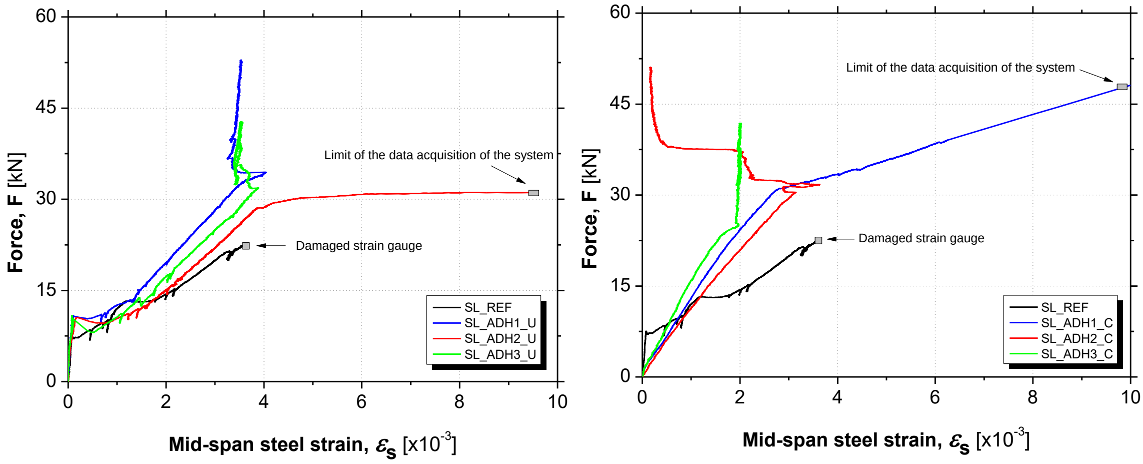

(a) (b)

Figure 5 – Force *vs.* mid-span steel strain obtained on the (a) uncracked and (b) pre-cracked series

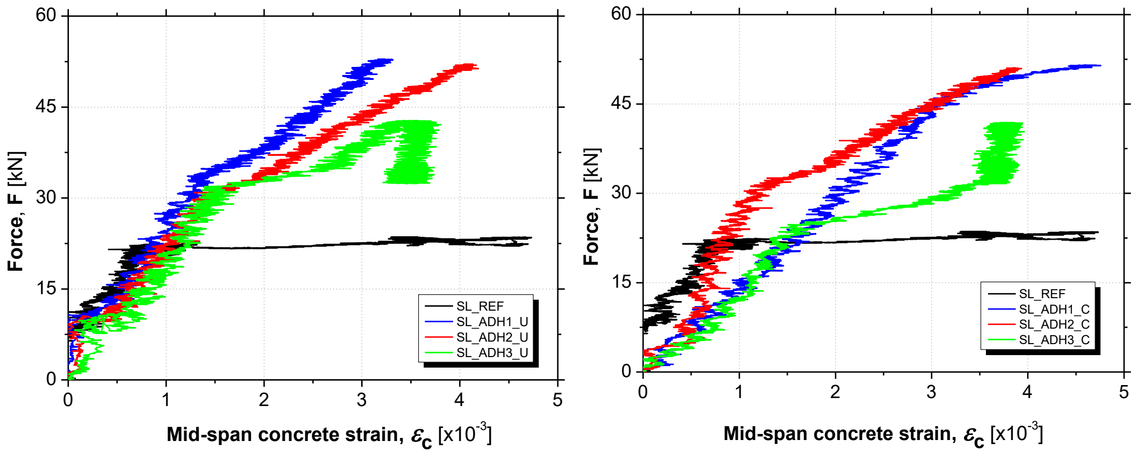

(a) (b)

Figure 6 – Force *vs.* mid-span concrete strain obtained on the (a) uncracked and (b) cracked series.

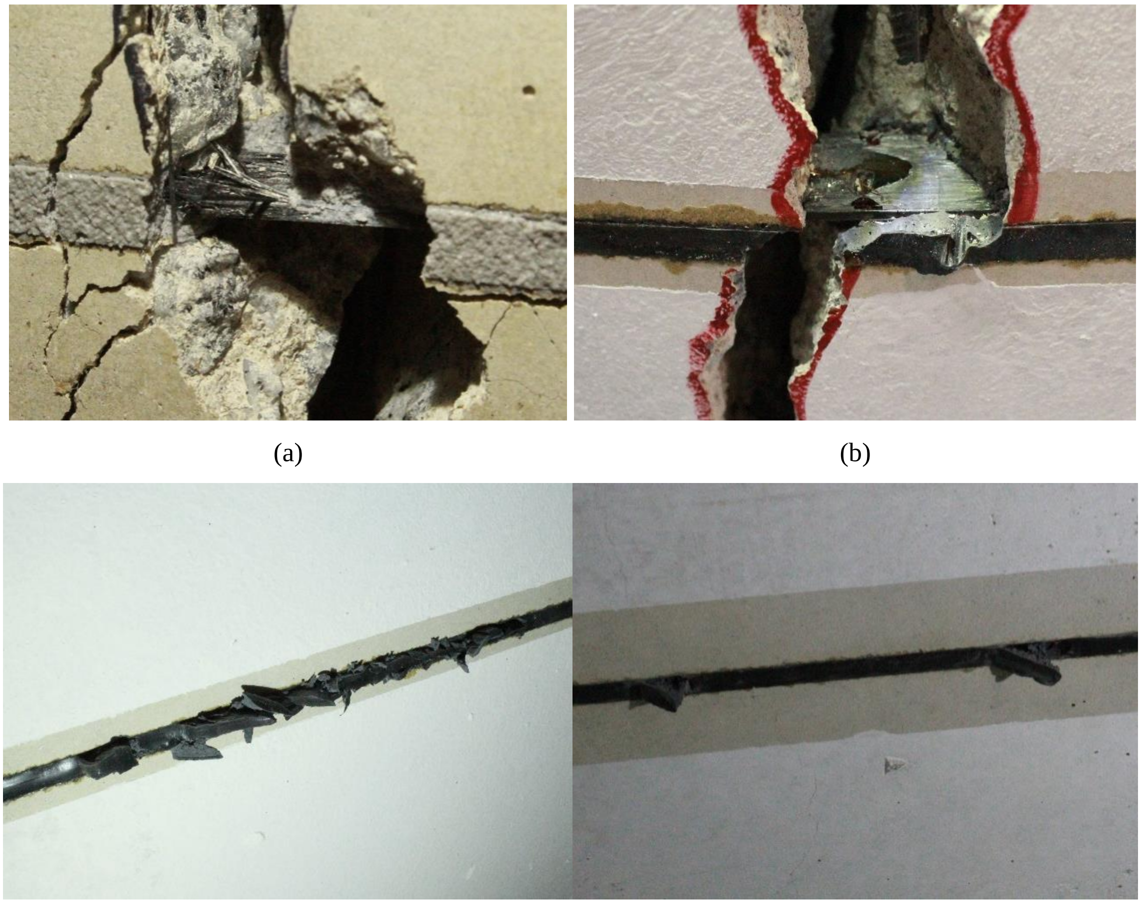

(a) (b) (c) (d)

Figure 7 – Failure modes: (a) CFRP laminate failure (SL_ADH1 and SL_ADH2); (b) debonding at laminate-adhesive interface (SL_ADH3); (c) cohesive failure of ADH3 at the ends of the strengthening system (SL_ADH3); (d) cohesive failure of the adhesive between the mid-span section and the ends of the strengthening (SL_ADH3).

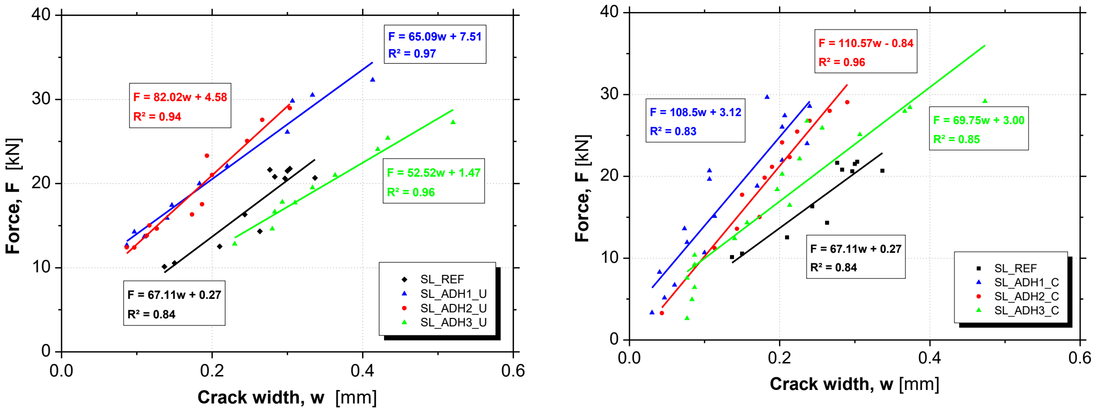

(a) (b)

Figure 8 – Crack width evolution on the (a) cracked and (b) uncracked series.

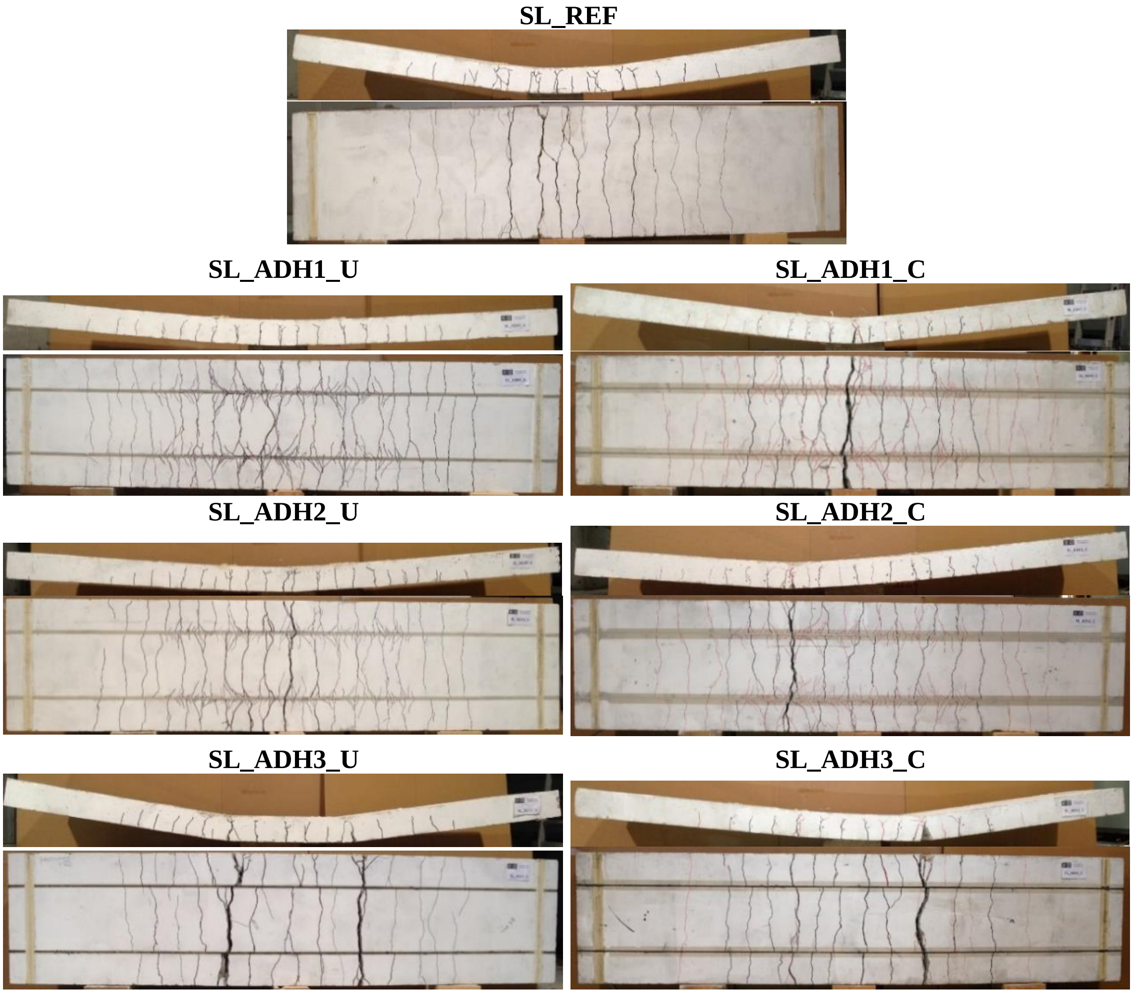

Figure 9 – Crack pattern of each slab after the test on lateral and bottom surfaces. Notes: on reference and uncracked slabs, the cracks were marked using black colour; on the cracked slabs, the cracks caused by the pre-cracking process were marked with red colour and the cracks resulting of the test up to failure were marked using black colour.

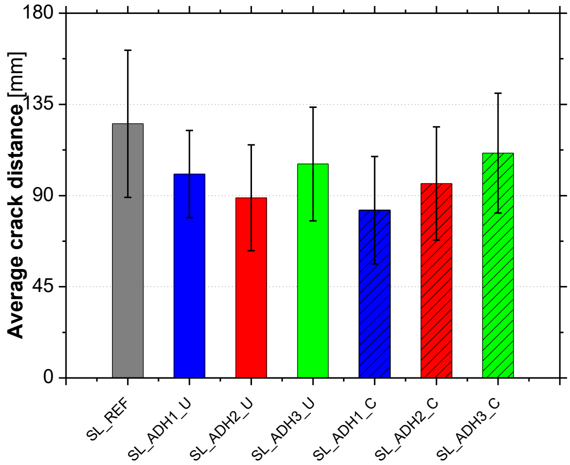

Figure 10 – Average crack distance of each slab.

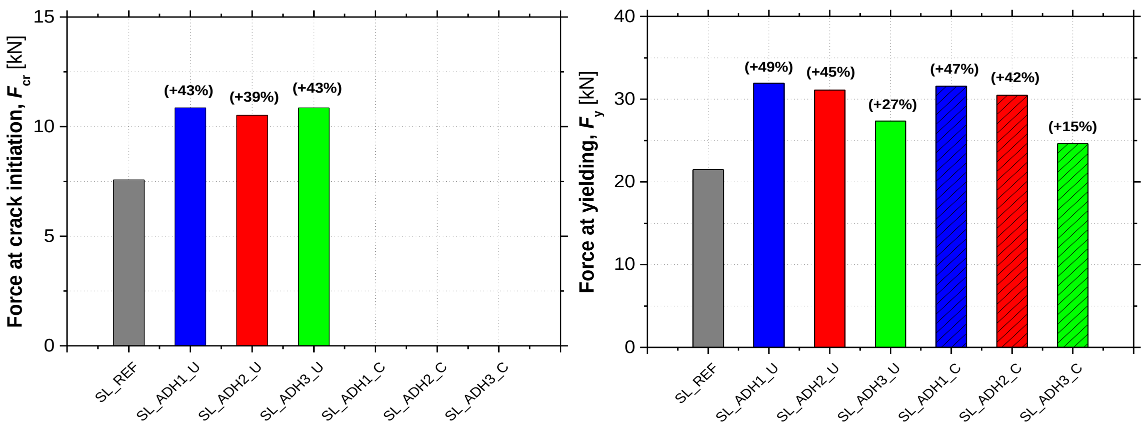

(a) (b)

Figure 11 – Force at: (a) crack initiation; (b) bottom steel yielding. Notes: the values between parentheses are the percentage increase to SL_REF at this phase of the test.

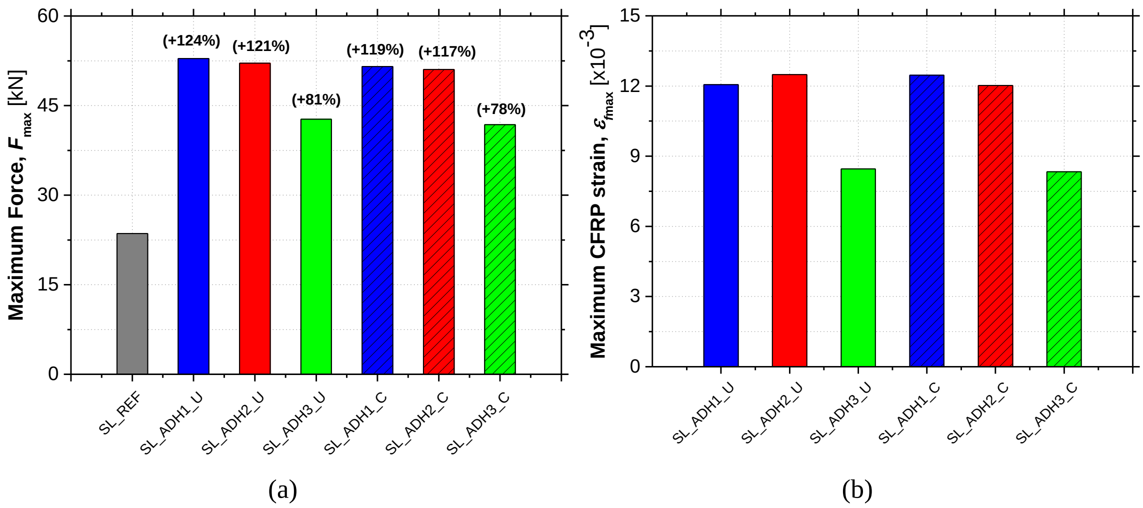

Figure 12 – Maximum force (a) and maximum CFRP strain (b). Note: the values between parentheses are the percentage increase to SL_REF at this phase of the test.

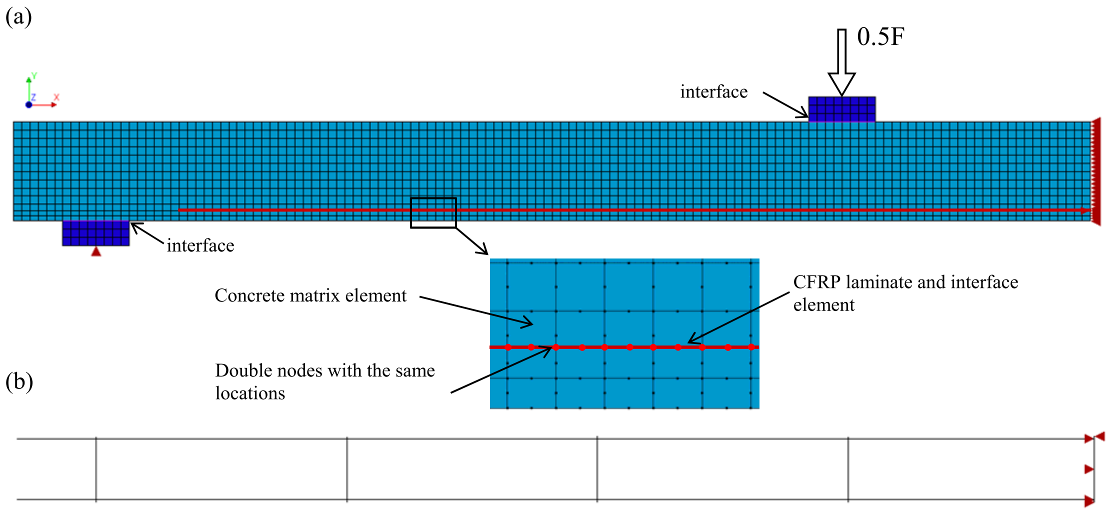

Figure 13 – Finite element model adopted for the simulation of the slabs: (a) concrete and laminate, (b) steel reinforcement.

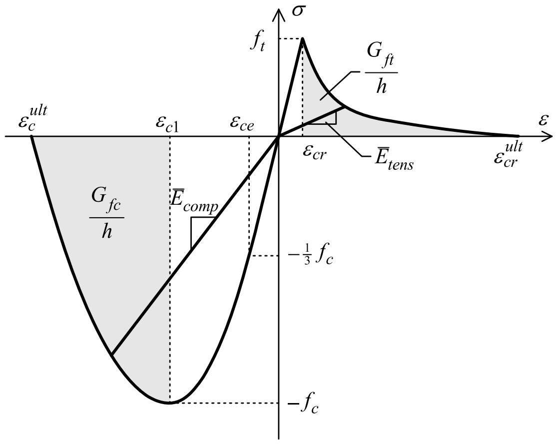

Figure 14 – Uniaxial stress-strain relationship for concrete.

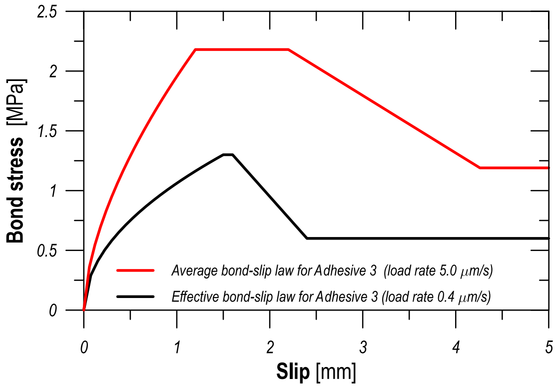

Figure 15 – Comparison of bond-slip laws for Adhesive 3, average according to DPT (red line) [22], effective (black line).

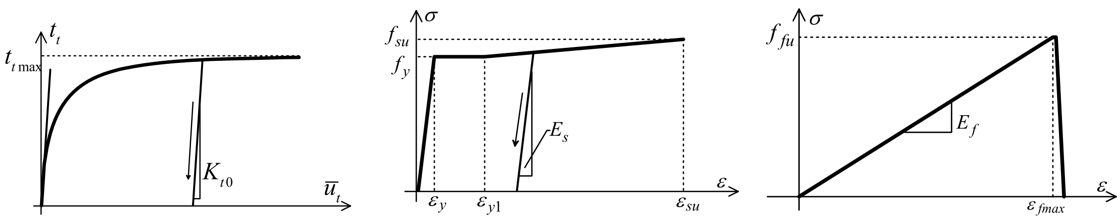

(a) (b) (c)

Figure 16 – (a) bond-slip law for steel reinforcement, (b) stress-strain relationship for steel reinforcement, (c) stress-strain relationship for CFRP laminate.

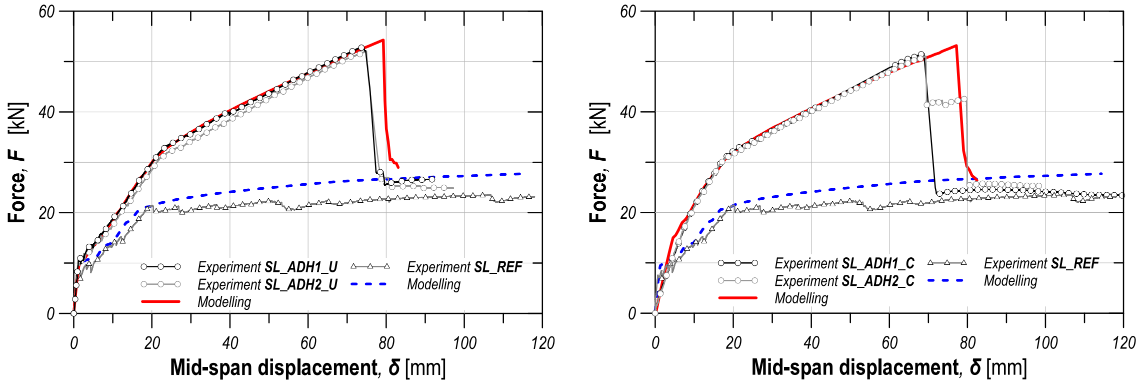

(a) (b)

Figure 17 – Comparison between experimental and numerical modelling of the load *vs*. displacement behaviour for slabs with stiff adhesives: (a) slabs uncracked before strengthening, (b) slabs preloaded and cracked before strengthening.

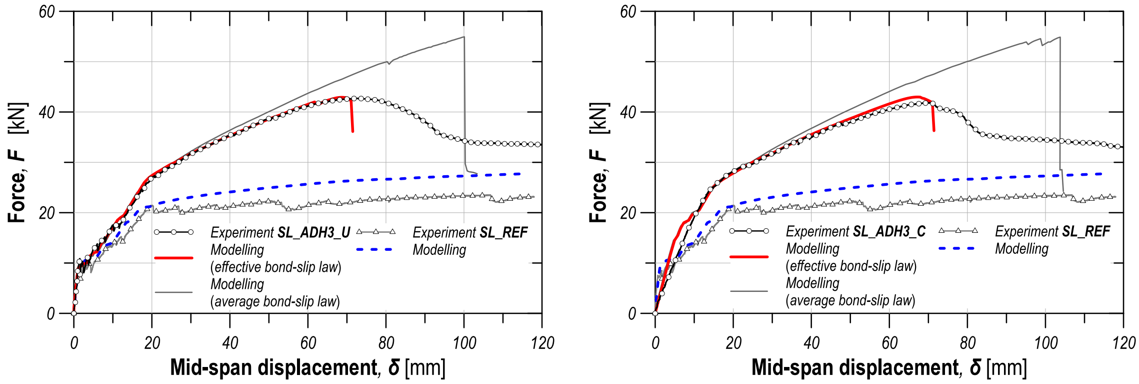

(a) (b)

Figure 18 – Comparison between experimental and numerical modelling of the load *vs*. displacement behaviour for slabs with flexible adhesive: (a) slab uncracked before strengthening, (b) slab preloaded and cracked before strengthening.

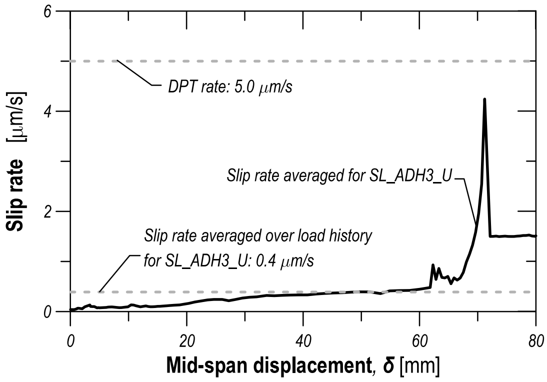

Figure 19 – Averaged slip rate between CFRP laminate and concrete for SL_ADH3_U slab.

(a)

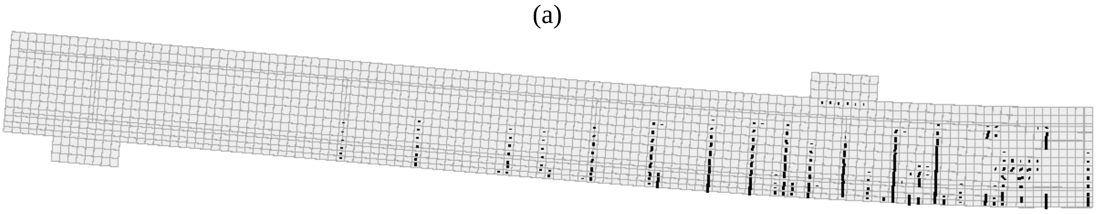

(b)

Figure 20 – Comparison between the experimental and numerical crack pattern for slab SL_ADH2_U.

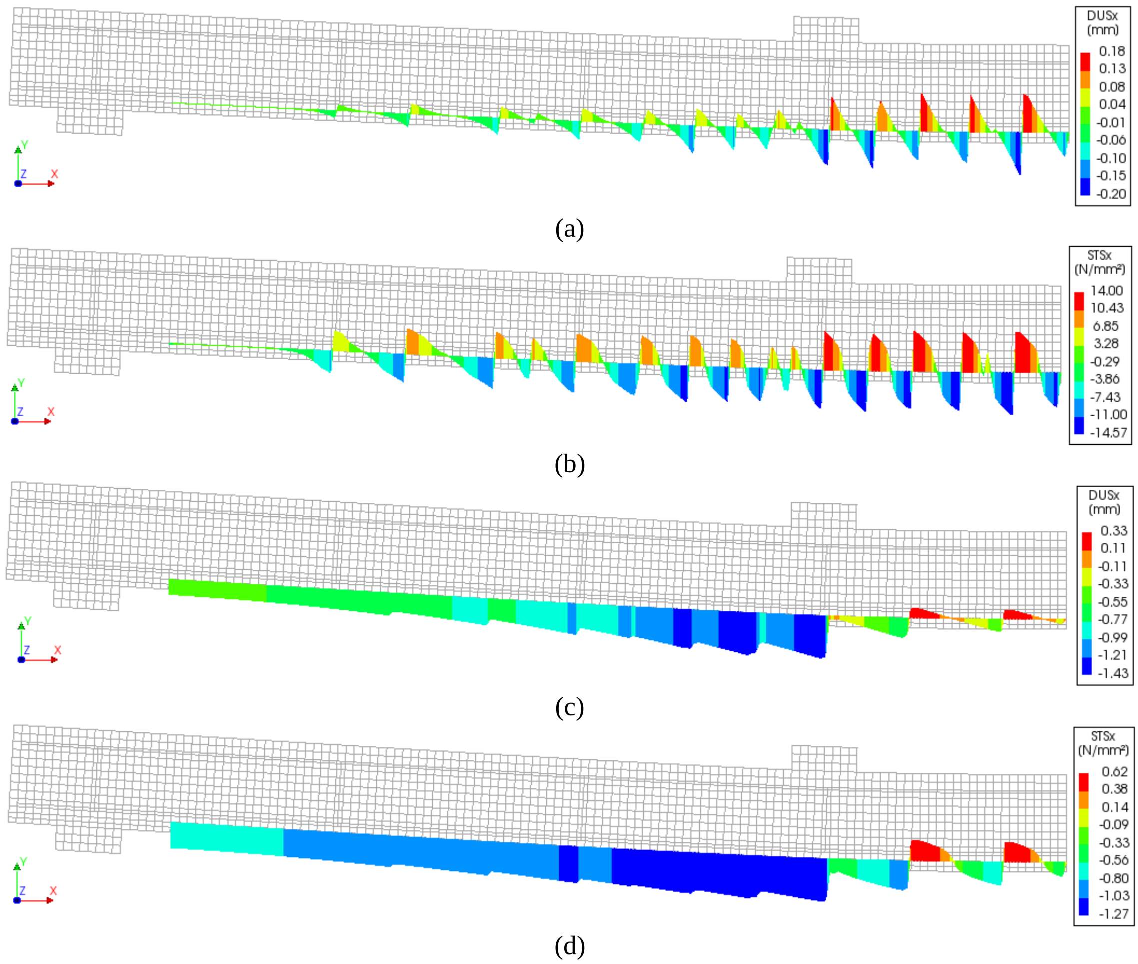

Figure 21 – Development of slips (a), (c) and bond stresses (b), (d) for slabs SL_ADH1_U (stiff adhesive) and SL_ADH3_U (flexible adhesive) – external load of 40 kN.